Article

Current Biology

Life-Long Neurogenic Activity of Individual Neural Stem Cells and Continuous Growth Establish an Outside-In Architecture in the Teleost Pallium

Graphical Abstract

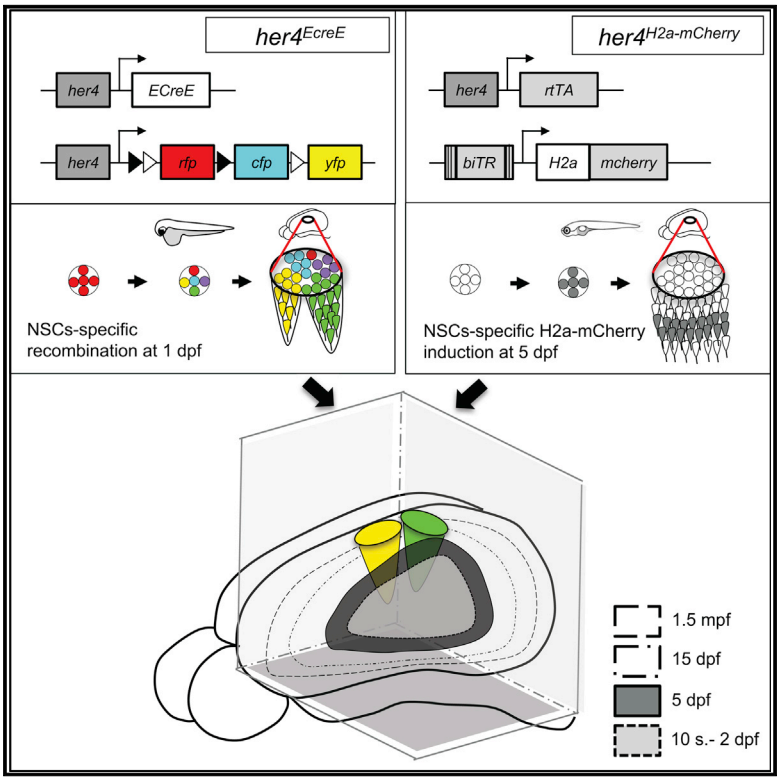

Highlights

- Neurons of the teleost pallium are arranged in concentric age-dependent layers
- Neurons of the central pallial domain, Dc, are born during embryogenesis
- Most pallial neurons are generated from ventricular *her4*-positive radial glia
- The majority of individual pallial radial glia are neurogenic throughout life

Authors

Giacomo Furlan, Valentina Cuccioli, Nelly Vuillemin, ..., Emmanuel Beaurepaire, Isabelle Foucher, Laure Bally-Cuif

Correspondence

isabelle.foucher@pasteur.fr (I.F.), laure.bally-cuif@pasteur.fr (L.B.-C.)

In Brief

Furlan et al. investigate the spatiotemporal events building the zebrafish pallium. Their "3D + birthdating time" map reveals an outside-in organization where neurons order in age-dependent sheets and where most individual neural stem cells are neurogenic life long. This strategy suggests a possible basal layout for pallial diversification.

Furlan et al., 2017, Current Biology *27*, 3288–3301
November 6, 2017
https://doi.org/10.1016/j.cub.2017.09.052

CellPress

Current Biology
Article

Life-Long Neurogenic Activity of Individual Neural Stem Cells and Continuous Growth Establish an Outside-In Architecture in the Teleost Pallium

Giacomo Furlan,[1,6] Valentina Cuccioli,[1,2,3,7] Nelly Vuillemin,[4,8] Lara Dirian,[1,9] Anna Janue Muntasell,[5] Marion Coolen,[1,2,3] Nicolas Dray,[1,2,3] Sébastien Bedu,[1,2,3] Corinne Houart,[5] Emmanuel Beaurepaire,[4] Isabelle Foucher,[1,2,3,*] and Laure Bally-Cuif[1,2,3,10,*]

[1]Team Zebrafish Neurogenetics, Paris-Saclay Institute for Neuroscience (Neuro-PSI), UMR 9197, CNRS-Université Paris-Sud, Avenue de la Terrasse, 91190 Gif-sur-Yvette, France
[2]Unit Zebrafish Neurogenetics, Developmental and Stem Cell Biology Department, Institut Pasteur, 25 Rue du Dr Roux, 75015 Paris, France
[3]CNRS UMR 3738, 25 Rue du Dr. Roux, 75015 Paris, France
[4]Laboratory for Optics and Biosciences, École Polytechnique, CNRS UMR 7645 and INSERM U1182, 91128 Palaiseau, France
[5]Centre for Developmental Neurobiology and MRC Centre for Neurodevelopmental Disorders, IoPPN, King's College London, London SE1 1UL, UK
[6]Present address: CRCL, UMR INSERM 1052, CNRS 5286, Centre L. Bérard, 28 Rue Laennec, 69008 Lyon, France
[7]Present address: Qiagen, 3 Avenue du Canada, LP809, 91974 Courtaboeuf Cedex, France
[8]Present address: Centre de Recherche CERVO, Québec City, QC, Canada
[9]Present address: ESTEAM Paris-Sud, CNRS U935, 7 Rue Guy Moquet, 94805 Villejuif, France
[10]Lead Contact
*Correspondence: isabelle.foucher@pasteur.fr (I.F.), laure.bally-cuif@pasteur.fr (L.B.-C.)
https://doi.org/10.1016/j.cub.2017.09.052

SUMMARY

Spatiotemporal variations of neurogenesis are thought to account for the evolution of brain shape. In the dorsal telencephalon (pallium) of vertebrates, it remains unresolved which ancestral neurogenesis mode prefigures the highly divergent cytoarchitectures that are seen in extant species. To gain insight into this question, we developed genetic tools to generate here the first 4-dimensional (3D + birthdating time) map of pallium construction in the adult teleost zebrafish. Using a Tet-On-based genetic birthdating strategy, we identify a ''sequential stacking'' construction mode where neurons derived from the zebrafish pallial germinal zone arrange in outside-in, age-related layers from a central core generated during embryogenesis. We obtained no evidence for overt radial or tangential neuronal migrations. Cre-lox-mediated tracing, which included following Brainbow clones, further demonstrates that this process is sustained by the persistent neurogenic activity of individual pallial neural stem cells (NSCs) from embryo to adult. Together, these data demonstrate that the spatiotemporal control of NSC activity is an important driver of the macroarchitecture of the zebrafish adult pallium. This simple mode of pallium construction shares distinct traits with pallial genesis in mammals and non-mammalian amniotes such as birds or reptiles, suggesting that it may exemplify the basal layout from which vertebrate pallial architectures were elaborated.

INTRODUCTION

The dorsal telencephalon (pallium) of vertebrates is involved in complex sensory processing and cognitive operations. It derives from homologous developmental territories between species, which also partly share pallial organization and connectivity but display huge variations in pallial morphology. How this diversity in morphology has arisen such that species-specific adult cytoarchitectures can be constructed from the same set of developmental genes and fields to achieve similar functions is not fully understood.

There are several potential drivers of species-specific variations in brain size and architecture, such as the spatiotemporal control of progenitors' neurogenic activity, neurogenesis lineages, neuronal migration, or neuronal death. The relative contribution of these events to pallium construction has been best studied in the neocortex of mammals and its homologous pallial territory in birds and reptiles [1, 2]. In mammals, neural progenitor cells (NPCs) along the neocortical ventricular zone (VZ) are multipotent and sequentially produce distinct excitatory neuronal subtypes, either directly or through transient amplifying progenitors (TAPs) [3], following a chronological switch of fate determinants inside single NPCs [4–7]. When complemented by radial migration, this process generates a layered functional organization of excitatory neurons reflecting neuronal birthdate, ordered from deep (old) to upper (young) layer identities in an ''inside-out'' pattern [8] (Figure S1Aa). Classically, layer 4 (L4) neurons receive thalamic afferents and, together with upper-layer neurons, are involved in intra-cortical circuitries, whereas deep layers (L5) host projection neurons.

The temporal regulation of encoding neuronal subtypes by NPCs is shared between amniote species [9, 10]. However, the macro-organization of the pallium differs strikingly between mammalian and non-mammalian amniotes. In birds and reptiles,

the pallial domain develops from a progenitor field homologous to the neocortex [11, 12], contains identical neuronal subtypes, is involved in similar circuitries [13–15], and is largely organized in functional fields or nuclei (Figures S1Ab and S1Ac) [2]. In birds, distinct regulation of neurogenesis timing (on- and offset times) was observed along the medio-lateral axis of the developing pallial VZ [9]. Because neuronal identities are birthdate dependent, this could generate differently sized and functionally specialized nuclei as opposed to layers [9] (Figure S1Ab)—although whether this occurs within individual functional networks is unclear [15]. The reptilian neocortex, in its dorsal sector, exhibits a three-layered laminar structure, generated in a radial outside-in pattern during a brief temporal window [10, 16]. The relative positions of L4 and L5 neuronal fields are also suggestive of spatial restrictions in NPC activities along the VZ (Figure S1Ab) [10, 15]. Overall, it has proven difficult to infer from these comparisons what could be the ancestral strategy involved in building neocortical (or, more generally, pallial) architecture.

We identify here the spatiotemporal events driving pallium construction in the teleost zebrafish as a representative of a more distant anamniote non-tetrapod vertebrate. This first "3D + birthdating time" pallial neuronal map reveals an outside-in organization where neurons order in age-dependent sheets and where most individual NPCs are neurogenic throughout their lifetime. This globally simple strategy of pallium construction bears reminiscence with mechanisms in amniotes, and its simplicity suggests a possible basal layout for the elaboration of pallial diversification.

RESULTS

Proliferation and Neurogenic Activities in the Zebrafish Pallium Are Largely Restricted to Ventricular Radial Glia

Ray-finned fish (actinopterygians) all have an everted pallium leading to positioning the VZ, which contains NPC bodies, at the surface of the hemispheres [17]. The ventricle is enclosed by a stretching sheet of cells derived from the roof plate, the tela choroida, attached to the base of the everted folds (Figure S1B). To analyze the ontogeny of the zebrafish adult pallium, we first characterized the proliferation and neurogenic activities of NPCs along the pallial VZ from embryonic to adult stages. The neurogenic population in this territory is essentially composed of radial glial cells (RGs), identified by their expression of *Glial Fibrillary Acidic Protein* (*gfap*) [18], glutamine synthase (GS) [19, 20], and the transcription factor-encoding gene *her4*/*Hes5* [21]. As previously documented, NPCs cover the entire VZ from embryonic to adult stages (Figures S1D–S1G), and exhibit life-long proliferative activity, measured with the Proliferating Cell Nuclear Antigen (PCNA) marker (Figure S2) [18]. This differs from pallial neurogenesis in amniotes [22–24]. RG proliferation along the zebrafish pallial VZ nevertheless decreases from juvenile stages to adulthood (Figures S2B–S2E) [21, 25]. During neocortex developmental neurogenesis in mammals, but not in most non-mammalian amniotes, there is an amplification step via intermediate progenitors, forming a recognizable sub-VZ [10, 26, 27]. These NPCs are non-glial but proliferative. To examine this issue in zebrafish, we compared PCNA expression with RG markers from 2 days post-fertilization (dpf) to 3 months post-fertilization (mpf). At all times, PCNA expression in the pallium was largely limited to RGs themselves, failing to indicate a non-RG, proliferating sub-VZ (Figure S2, insets). We previously reported that lineage amplification from RGs is limited in adults [28]; thus, this property extends to the stages of pallium construction.

In the following section, "NPCs" (versus RGs) will refer to the population of neural progenitors as a whole (RG + intermediate progenitors), or to a neural progenitor whose nature was not precisely defined.

H2a-mCherry Retention Is a Suitable Birthdating Strategy in the Zebrafish Pallium

We reasoned that, in light of the minimal amplification exhibited by neurogenic lineages in the zebrafish pallium, we should be able to use a retention assay as a neuronal birthdating strategy. The Histone-fluo retention assay (a fluorescent reporter fused to stable Histone2a or H2b proteins) was efficiently used to study stem cell divisions in mammals [29, 30]. We thus developed an in vivo birthdating method based on Tet-On elements [31] that would lead to the expression of H2a-mCherry upon induction. In the driver line *Tg(her4:rtTA, GFP:cmlc2)*, the *her4*/*Hes5* NPC-specific promoter drives expression of *reverse tetracycline-controlled transcriptional transactivator* rtTA with a Flag epitope (Figure 1A). This line faithfully drives *rtTA* expression in all pallial RGs (Figure S3A). In the reporter line *Tg(GFP:biTRE:H2amCHERRY, crist:Venus)*, the *bidirectional tetracycline responsive element* biTRE drives expression of both GFP and an H2a-mCherry fusion protein (Figure 1A).

We induced rtTA activity in double-transgenic animals by a 9-*tert*-butyldoxycycline (9TB) treatment [32]. No leaky H2A-mCherry expression was detected without 9TB (not shown). Upon 9TB application, H2A-mCherry was selectively induced in RGs at all stages (Figures S3C–S3G). One day after treatment, most RGs (ventricular GFP-positive, Flag-positive cells) expressed high levels of H2a-mCherry, indicating efficient induction (Figures S3C–S3G). Induction frequency was homogeneous along the antero-posterior axis, 80% of VZ cells being H2a-mCherry positive at anterior, middle, and posterior pallial levels after a treatment at 5 dpf (Figure S3B). At 1.5 mpf, however, induction appeared less efficient in the medial domain of Dl (Figure S3G, red asterisk). Together, this strategy allowed us to pulse-label RGs with H2a-mCherry at all stages, and perform fate tracking at the population level.

A birthdating method implies that the tracer highlights cells generated within a restricted number of cell divisions following induction. Therefore, a non-dividing RG should retain its initial mCherry staining, whereas daughter cells of a dividing RG should inherit half its mCherry content, progressively diluting out the label. Low amounts of 9TB and short chase times were used to validate these dilution properties on polyclones induced at 1 dpf and analyzed at 5 dpf (Figure 1B). The amount of mCherry per nucleus was inferred from summing mCherry fluorescence staining intensity over the whole nucleus volume, measured using Imaris software. We observed a 2-fold dilution of the mCherry content after each division (Figure 1B). Finally, we verified that label-retaining cells in our system were indeed mainly neurons: after 9TB treatment at 1 dpf and a 4-day chase, all mCherry-positive cells were positive for the neuronal marker HuC/D (Figure 1C). Thus, the neurons generated after few divisions from transiently induced *her4*-positive pallial RGs retain

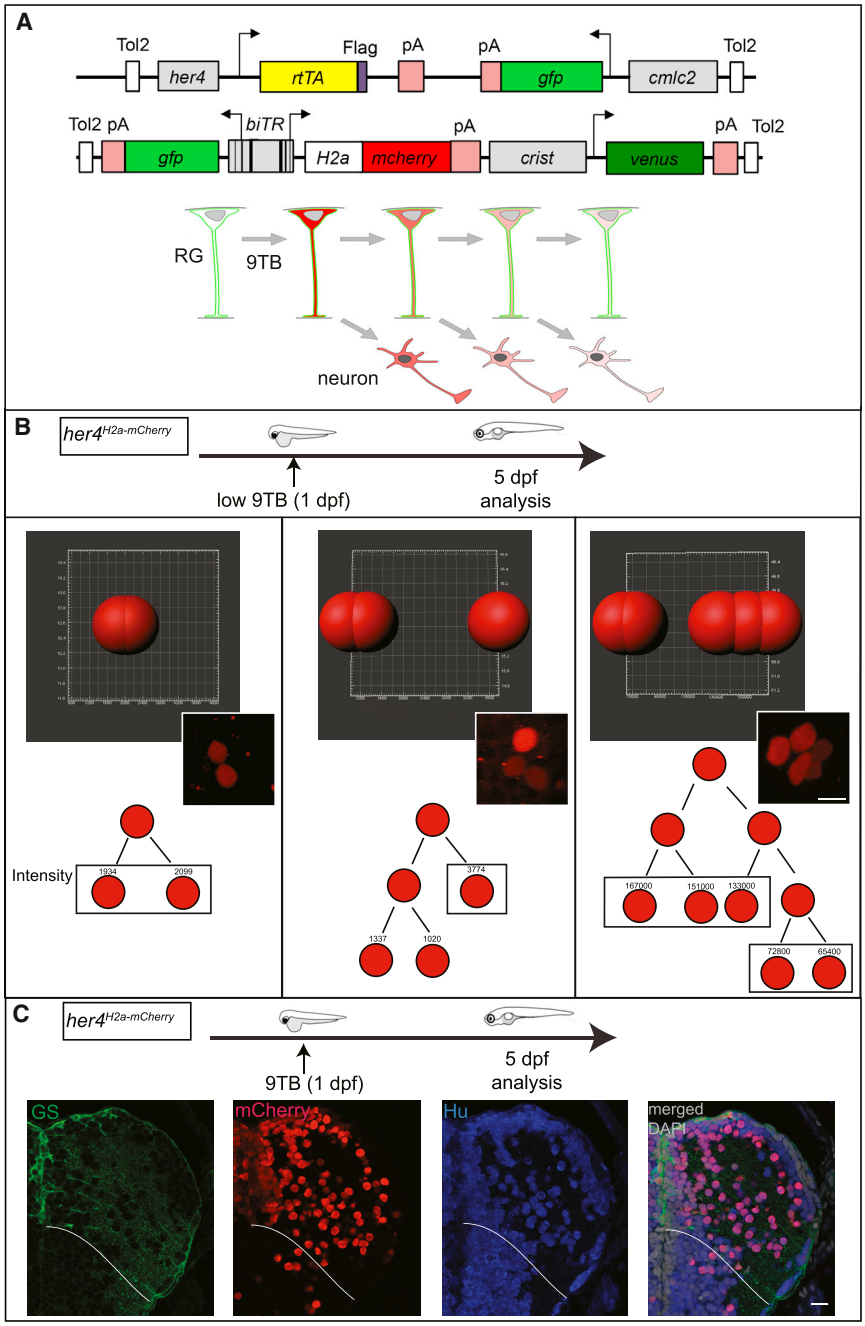

Figure 1. Neuronal Birthdating from *her4*-Expressing RGs In Vivo

(A) Genetic strategy. Top: 9-*tert*-butyldoxycycline (9TB) triggers stable H2a-mCherry and transient GFP activation in *her4*-positive RGs in double-transgenic animals for the depicted constructs. Bottom: neurons generated by the first RG (top, green) divisions following 9TB induction inherit detectable levels of H2a-mCherry (red). The label is lost upon successive divisions.

(B) Imaris quantification of mCherry immunostaining in 2- (left; n = 6), 3- (middle; n = 2), or 5- (right; n = 1) cell clones from different $her4^{H2a\text{-}mCherry}$ animals pulsed with 9BT at 1 dpf and analyzed at 5 dpf. Top: Imaris segmentation of mCherry-positive cells in individual clones. Middle: corresponding photomicrograph. Bottom: reconstructed lineage trees and fluorescence intensities. Scale bar, 7 μm.

(C) Neuronal fate of the mCherry-labeled daughter cells of *her4*-positive RGs in $her4^{H2a\text{-}mCherry,9BT(1dpf)}$ fish analyzed at 5 dpf. Triple immunocytochemistry for GS, mCherry, and HuC/D on a pallium cross-section (one hemisphere). White lines indicate pallial-subpallial boundary. Scale bar, 10 μm.

See also Figures S1–S3. Abbreviation definitions can be found in Figure S1B.

H2a-mCherry, and the time of 9TB application is a proxy for their birthdate.

Pallial Neurogenesis Follows a Sequential Stacking Process

We timed neuron generation from *her4*-positive pallial RGs at embryonic, larval, and juvenile stages (10 somites, 1–2–5–15 dpf and 1.5 mpf) in *Tg(her4:rtTA);Tg(GFP:biTRE:H2a-mCherry)* double-transgenic animals (hereafter referred to as $her4^{H2a\text{-}mCherry,9TB(t)}$ for a 9TB induction at time t). To position these neurons within the adult pallium, we first analyzed a mid-antero-posterior level, identified by the joint presence of the dorsal sulcus ypsiloniformis (sy) and the lateral sulcus (ls) (Figure S1B). Co-immunostaining of mCherry with parvalbumin (PV) together with the sulci landmark helped identify neuroanatomical territories: the lateral pallium (Dl) (containing PV-positive neuronal cell bodies), the medial pallium (Dm) (located medial to sy), and a deep domain recognized as Dc (enriched in PV projections) [33] (Figure S1B; Figure 2A′).

Early 9TB treatments (10 somites, 1–2 dpf) generated mCherry-positive neurons positioned deep into the pallial parenchyma, close to the pallial-subpallial boundary (Figures 2A–2B′), in a domain overlapping with Dc. In $her4^{H2a\text{-}mCherry,9TB(5dpf)}$ animals, the mCherry-positive domain partly overlapped with this earlier-generated territory in medial locations but was otherwise positioned more dorsally and laterally and precisely surrounded Dc, including neurons in the deepest regions of Dm, Dl, and Dp (Figures 2C–2D′; Figures S4M and S4N). With increasing induction stages (15 dpf and beyond), concentric horseshoe domains were again progressively displaced to more medial, dorsal, and lateral positions (Figures 2C–2E′). The neurons generated at late stages (1.5 mpf) formed the most superficial area of the pallium (Figures 2F and 2F′). The paucity of neurons generated at 1.5 mpf in the most dorsal aspect of the pallium is consistent with a lower efficacy of 9TB induction in this area at this late stage (Figure S3G). The narrow territory built by pallial neurons

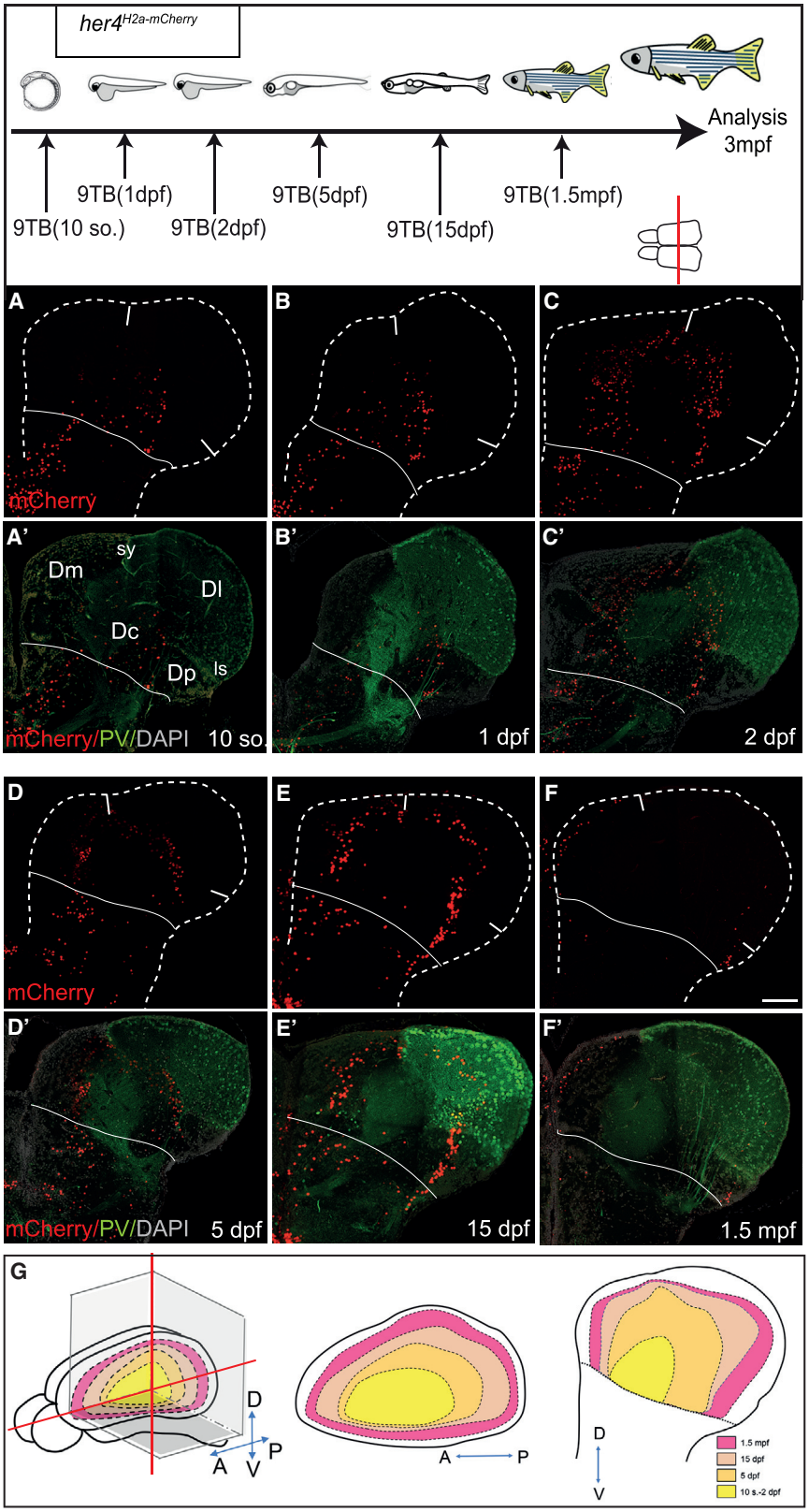

Figure 2. Zebrafish Pallial Neurogenesis Follows a Sequential Stacking Process: Medio-lateral Analysis

Top: experimental design.

(A–F′) Distribution of mCherry-positive neurons (A–F) born from *her4*-positive RGs in *her4*$^{H2a\text{-}mCherry}$ induced with 9TB at the stages indicated. Cross-sections at 3 mpf at mid-antero-posterior levels, the level indicated by a red line on telencephalon dorsal view, are co-labeled for parvalbumin (PV; A′–F′). Solid white lines indicate pallium-subpallium boundary. Scale bar, 50 μm.

(G) Color-coded map of the position in the adult brain (left: "open" whole-mount view; middle: horizontal section; right: cross-section) of the neurons born from *her4*-positive RGs at the stage indicated.

See also Figure S4.

between 1.5 and 3 mpf also shows that neurogenesis slows down after 1.5 mpf.

These data demonstrate the existence of an overall centrifugal gradient of neurogenesis in the zebrafish pallium, with the following characteristics: (1) it originates from the deepest territory of the adult pallium, in the position of Dc and the deepest neurons of Dm, Dl, and Dp: Dc and ventrally located pallial neurons form a "core" generated at embryonic stages; (2) it progresses in the dorsal and lateral directions (and medially at least starting at 15 dpf), neurons assembling around the core domain in progressively more superficial layers with time; and (3) it deposits neurons that arrange in an outside-in manner according to their birthdate with little or no radial mixing dorsally and laterally from the core. We postulate that pallial neurons simply sequentially stack over time as they delaminate from the VZ, contributing to pallial growth, in parallel to the enlargement of the germinal zone through symmetric RG divisions [28].

To understand pallium construction in 3D, systematic analyses were conducted at different antero-posterior levels, as well as on horizontal sections and whole-mount cleared preparations, with similar conclusions (Figure 3;Figures S4A–S4L and S5A). For example, at most anterior levels, mCherry-positive neurons only appeared in *her4*$^{H2a\text{-}mCherry,9TB(15dpf)}$ animals and later (Figures 3A–3D′). Taken together, our data indicate that the general logic of pallium construction is a 3-dimensional sequential stacking process where neurogenesis progresses dorsally and laterally, but also toward the anterior and posterior, from the central "core" domain over time (Figure 2G).

The *her4*-Positive RG Population Is Neurogenic throughout Life

To determine whether the same *her4*-positive RG population is neurogenic at all stages—or, in contrast, whether distinct RG subsets expressing *her4* at the time of induction are transiently neurogenic—we used conditional Cre-mediated lineage tracing [21]. Double-transgenic fish for *her4:ERT2CreERT2* [34] and the ubiquitous reporter *ubi:switch (Tg(−3.5ubi:loxP-GFP-loxP-mCherry))* [35] were pulsed with 4-hydroxy-tamoxifen (4OHT) (hereafter *her4*$^{switch,T(t)}$ fish for tamoxifen treatment at time t) at increasing developmental stages from 10 somites to 1.5 mpf. This approach labels with mCherry all the neurons produced by RGs expressing *her4* at the time of 4OHT application, and tracks their neurogenic potential from the onset of treatment.

mCherry distribution was analyzed in the 3-mpf pallial parenchyma on median sections (equivalent to Figure 2). mCherry-labeled neurons occupied large domains extending from the VZ to a precise parenchymal boundary below which no neurons were stained (red line, Figure 4). The latter position recedes from deep to superficial as recombination is induced at later times, and is comparable to the layer hosting neurons born at the 4OHT treatment time (compare Figures 2A–2F′ with Figures 4A–4F). In the labeled domains, most neurons express mCherry (see also [21]). These observations indicate that, at the population level, pallial *her4*-positive RGs are constitutively neurogenic.

Individual *her4*-Positive Pallial RGs Are Neurogenic throughout Life

Neurogenesis in the mammalian neocortex is in part achieved by the constitutive neurogenic activity of individual RG progenitor cells throughout embryogenesis [4]. To further challenge the parallels between the mammalian and zebrafish neocortex, we asked whether individual zebrafish pallial RGs could sustain the entire neurogenesis process, here from 1 dpf to 3 mpf. We adapted Brainbow technology [36] [37] to visualize, in 3D, the contribution of unique embryonic RGs to the adult pallium. *her4:ERT2CreERT2;ubi:Zebrabow* double-transgenic embryos were mosaically recombined at 1 dpf. The corresponding adult telencephali were cleared and imaged in whole-mount view using a long-distance multiphoton confocal microscope, and clones were semi-automatically analyzed with single-cell resolution based on color ratios using Imaris (Figure 5A; Movie S1). 34 Brainbow clones (7,509 cells, from 8 pallial hemispheres) could be unambiguously mapped, including the coordinates of every constituent cell. For each individual clone, VZ cells versus neurons were counted—providing information on division mode and neurogenic activity—(Table S1), and the position of each clone was reported relative to neuroanatomical domains (schematically reconstructed in 3D from the manual segmentation of optical sections; Figure 5B) and on pallium dorsal views (Figures 5H and 5I).

Overall, the pallium appeared composed of clones of different sizes (29–654 cells), shapes, and compositions (Figures 5C–5G; Table S1). We identified 5 clone categories based on qualitative and quantitative criteria related to the neurogenic activity of their constituent NPCs. First, we distinguished clones "attached to" versus "detached from" the pallial VZ (Figures 5C–5E versus Figures 5F and 5G). Based on the sequential stacking model, the former clones identify active RGs whose neurogenic activity was continuous since its onset, whereas the latter identify RGs whose neurogenic activity was terminated before adulthood. Second, we quantitatively correlated pallial neuronal positions and neuronal birthdates (Table S2) and distinguished clones contributing to deep territories (containing neurons generated until 5 dpf) or, in contrast, confined to more superficial layers (Figures 5C, 5F, and 5G and Figures 5D and 5E, respectively). We found that "attached" clones all contained a significant number of VZ cells (Table S1), consistent with the frequent occurrence of RG-amplifying divisions already described in the adult [28]. Third, "attached" clones were largely predominant (n = 27, versus n = 7 "detached" clones). Finally, the majority of "attached" clones reached into deep pallial layers (Figure 5C; n = 16 clones of 25), 9 of them (56%) including Dc neurons (Table S1; Figure S5; Movie S2). Thus, there is a strong tendency for the neurogenic activity of individual pallial RGs to be continuous once initiated and, most remarkably, the majority of these RGs are neurogenic over an extended period of time, from embryonic stages until adulthood.

For confirmation, we backed up these results using classical Cre-lox tracing with low doses of 4OHT to obtain sparse labeling with 1–5 clones per telencephalic hemisphere, ensuring unequivocal clonality (Figures 6A and 6A′; Figure S5E–S5G). Double-transgenic fish for *her4:ERT2CreERT2* and the ubiquitous reporter *Tg(βactin:lox-stop-lox-hmgb1-mcherry)* [38] were pulsed at 5 dpf (*her4*$^{actswitch,T(5dpf)}$ fish) and analyzed at 1.5 mpf (Figures 6B–6D), allowing scoring 40 additional clones (Table S3) from 26 hemispheres. mCherry-positive clones were segmented in 3D using Imaris following triple immunofluorescence to detect quiescent RGs (GS-positive, PCNA-negative),

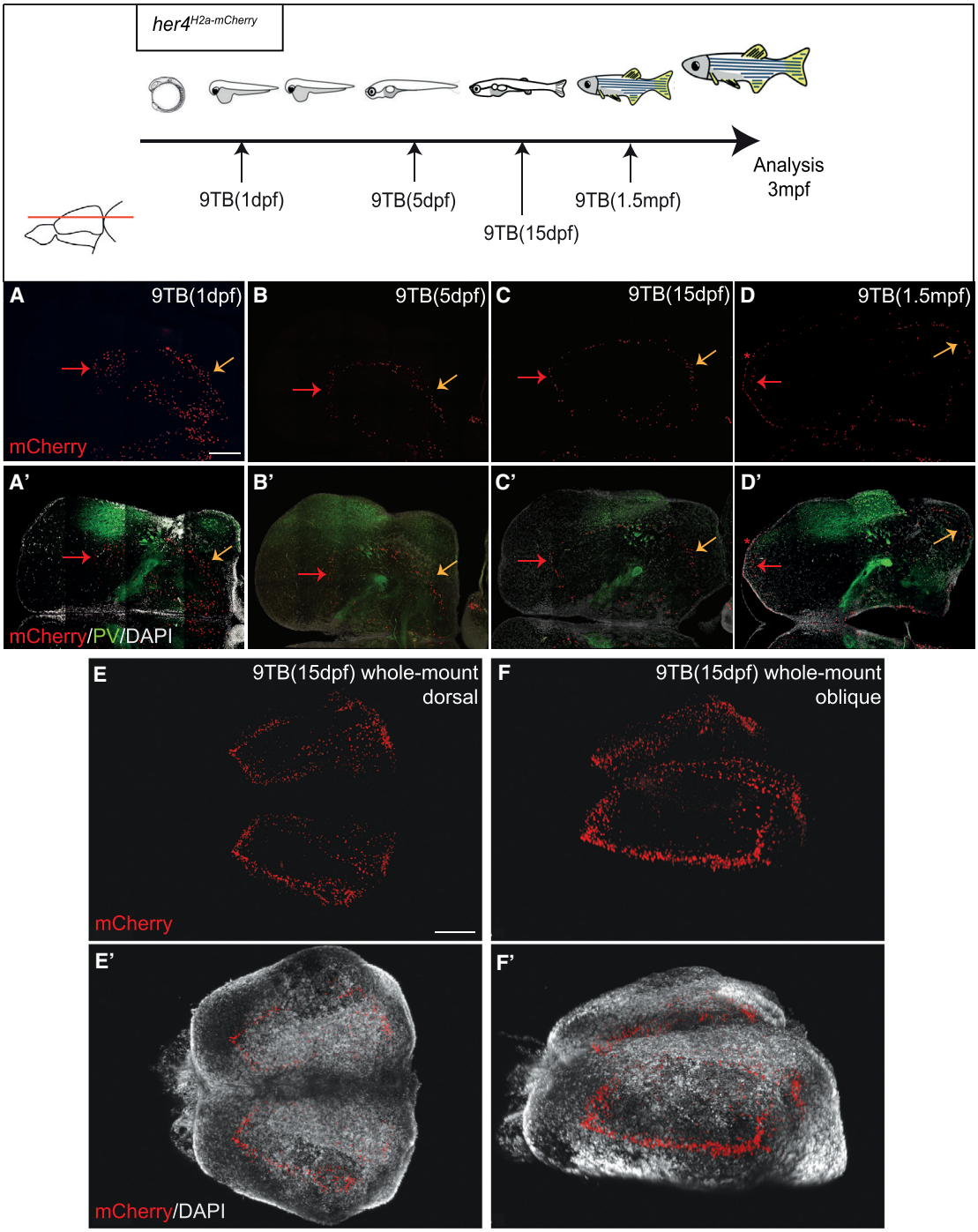

Figure 3. Zebrafish Pallial Neurogenesis Follows a Sequential Stacking Process: Antero-posterior Analysis

Top: experimental design.

(A–D′) Horizontal sections are shown and the level is indicated by a red line on telencephalon lateral view; same stainings as in Figures 2A–2F′. Red and orange arrows indicate anterior and posterior limits of the mCherry-positive neuronal layers, respectively. Red asterisks in (D) and (D′) indicate RGs maintaining the mCherry label.

(E–F′) Transparent whole-mount preparation of a *her4*$^{H2a\text{-}mCherry,9TB(15dpf)}$ pallium at 3 mpf. The pallium is observed from different angles (E: dorsal anterior left; F: lateral oblique).

Scale bars, 100 μm.

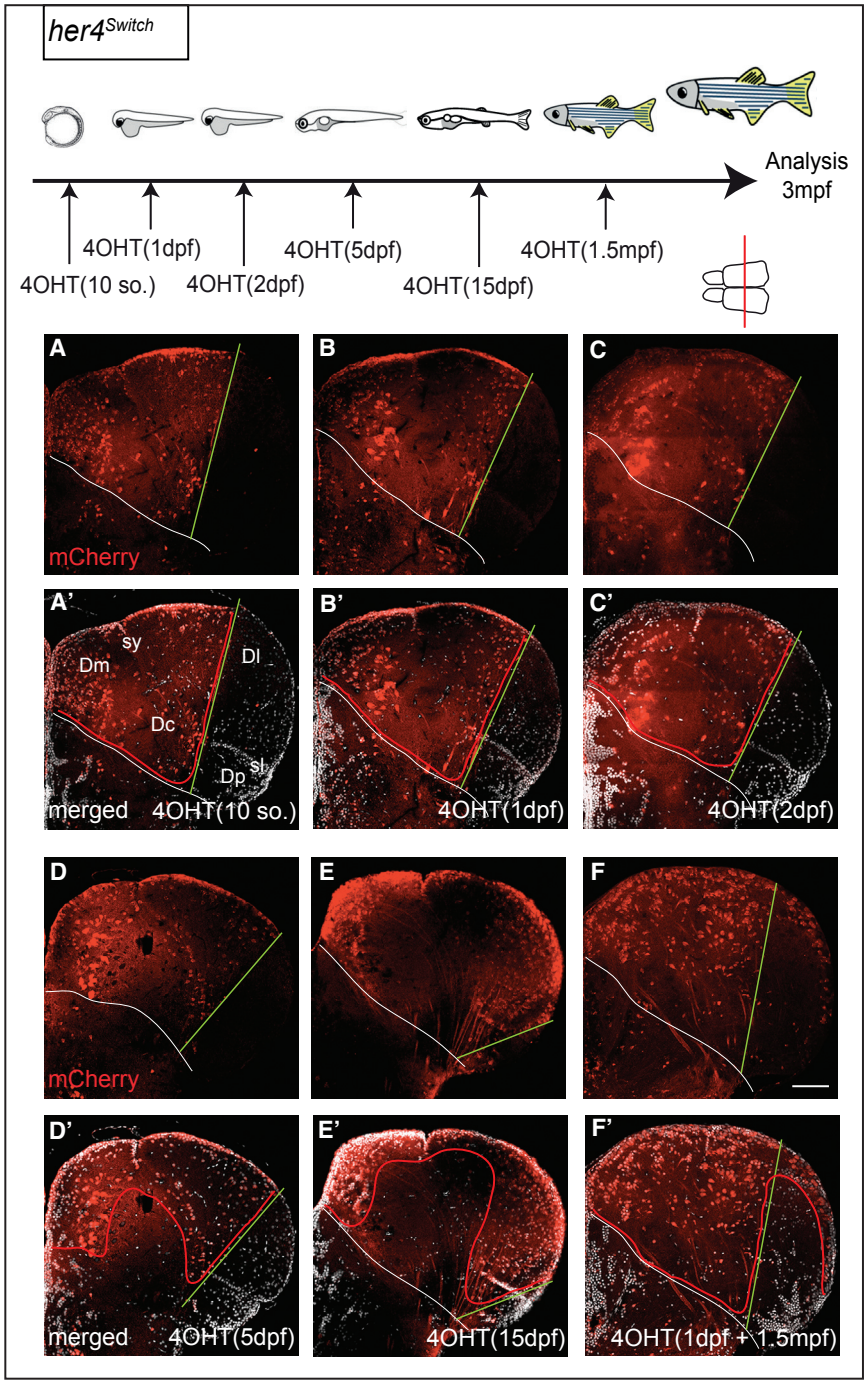

Figure 4. Continuous Neurogenesis from the Pallial *her4*-Positive RG Population

Top: experimental design. Distribution of mCherry-positive neurons (A–F) born from RGs that were *her4* positive at the time of 4OHT induction (stages at the bottom right of each panel). Cross-sections at 3 mpf are at identical mid-antero-posterior levels and the level is indicated by a red line on telencephalon dorsal view (A′–F′: mCherry and DAPI staining). Red lines indicate boundaries between territories with mCherry-positive and -negative neuronal cell bodies (mCherry is cytoplasmic in the *ubi:switch* line [35], and thus also stains processes). White lines indicate pallial-subpallial boundaries. Green lines delimit the recombined (Dm, medial part of Dl) and un-recombined (lateral part of Dl, Dp) pallial territories in *her4*^{switch} animals treated with 4OHT (see [21]; at any given time point, all pallial RGs are *her4* positive [Figure S2]; however, the pallial VZ expands laterally over time through the addition of RGs originating from a *her4*-negative source; therefore, the green lines shift toward the lateral with later recombination times). The *her4*^{switch} fish in (F) and (F′) was subjected to two consecutive inductions, at 1 dpf (medial neurons only, left to green bar limit) and then at 1.5 mpf (superficial neurons, right to green bar limit). Scale bar, 50 μm.

proliferating RGs (GS-positive, PCNA-positive), and the few intermediate progenitors (GS-negative, PCNA-positive) [18, 39] (Figures 6C and 6D). The recombination at 5dpf in this case precludes the recovery of "deep" clones (as defined in Figure 5); however, the same general clone types as defined in *her4*$^{Zebra-bow}$ fish were found using this method, with a large majority of "attached" clones (90%).

We next asked whether pallial neurogenesis modes from *her4*-positive RGs were subject to spatial variations along the antero-posterior and medio-lateral axes over time. We analyzed the spatial distribution across the VZ of the clone subtypes defined above (Figures 5H, 5I, 6E, and 6F). We also considered the proportion of symmetric versus neuron-generating divisions, inferred from the RG/neuron ratio within clones, and the presence or absence of intermediate progenitors (Tables S1 and S3). Although important clone-to-clone differences were observed, we found no bias in spatial distribution for either parameter, indicating that the net product of neurogenesis from individual *her4*-positive RGs is spatially homogeneous during pallium construction.

Birthdate-Independent Expression of Neuronal Subtype Markers in the Adult Zebrafish Pallium

Finally, we addressed the relationship between the topological organization of lineages and birthdates and neuronal identity. Except for the expression of regional markers in large areas [20, 33], the molecular identities of zebrafish adult pallial neurons are unknown. In rodent and human neocortex, several molecular markers are expressed in a lamina-specific manner [40]. For example, Ctip2, Fezf2, and ER81 are predominantly expressed by early-born L5 projection neurons [9, 41, 42], RORβ by L4 neurons [15], and Satb2, Mef2c, and Cux2 by late-born L2–L4 neurons [9, 15, 42, 43]. We established a list of "most informative candidates" based on shared expression in rodents and humans [44], notably at adult stage, and/or expression in functionally

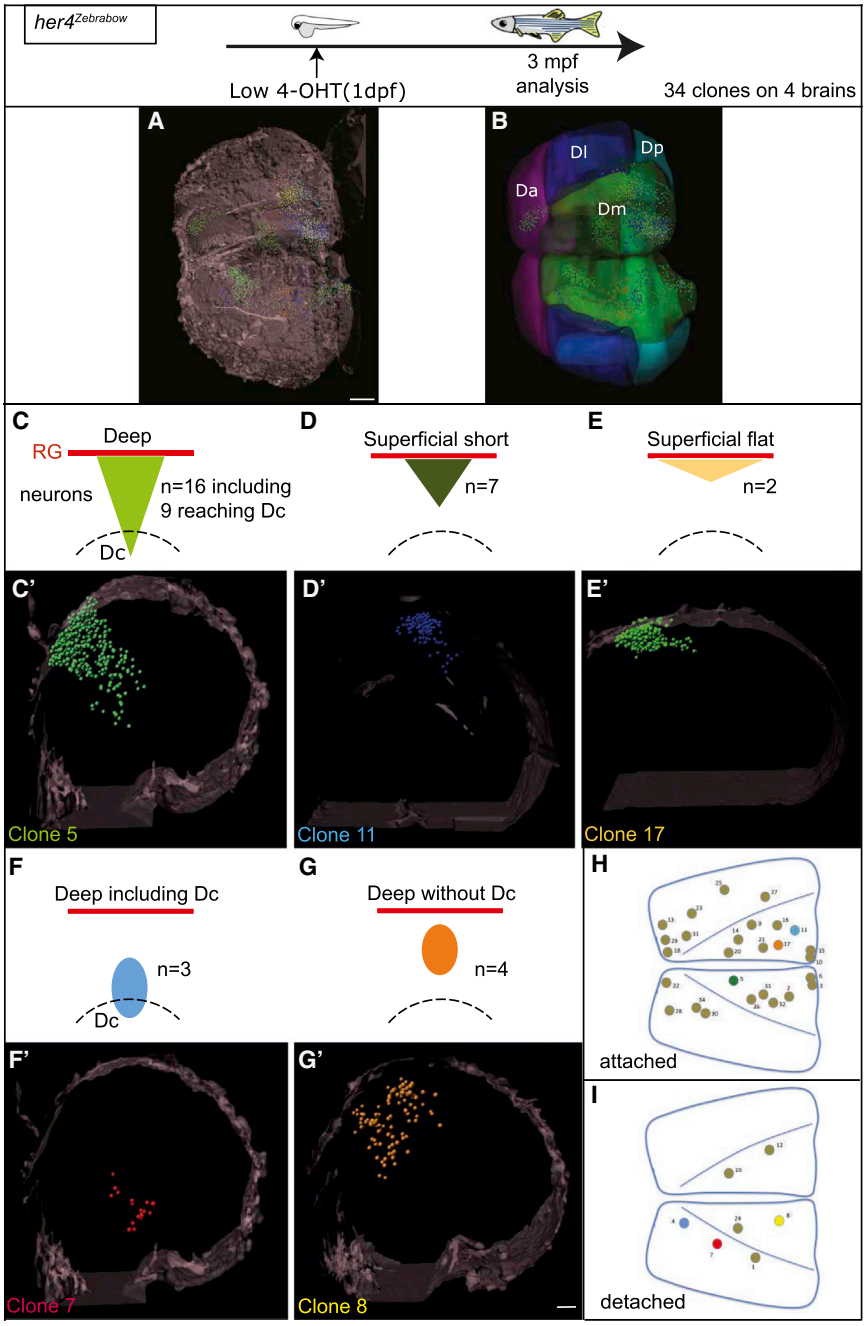

Figure 5. Individual Pallial RGs Are Neurogenic Lifelong

Top: experimental design.

(A) Whole-mount dorsal view (anterior left) of a 3-mpf pallium from a *her4*$^{Zebrabow,4OHT(1dpf)}$ fish, cleared and scanned. The position of individual cells of each clone is plotted (color coded). Brain surface (gray) was digitally added to help visualization. Scale bar, 150 μm.

(B) Corresponding location of pallial subdivisions.

(C–G′) Schematics (C–G) (red lines: RG layer; dashed lines: Dc limit) and thick optical cross-sections (C′–G′) of brains as in (A) highlighting the different categories of attached clones (C–E′) or detached clones (F–G′) (Table S1). "Deep" versus "superficial" clones contain neurons born before or at 5 dpf (Table S2).

(F–G′) Schematics (F and G) and thick optical cross-sections (F′ and G′) of brains as in (A) with examples of detached clones.

(H and I) Position of the 34 clones attached (H) or detached (I) on flattened dorsal views of the 3-mpf pallium.

Clones illustrated in (C′)–(G′) are colored. Scale bar, 80 μm. See also Figure S5, Tables S1 and S2, and Movies S1 and S2.

homologous pallial territories in birds [15], and conducted an in situ hybridization screen of adult brain slices (Figure 7; Figure S6; Table S4). Most marker genes were expressed within the zebrafish adult pallium, but their expression patterns were neither obviously layered nor did they form nuclei or cone-like clones. We could classify expression patterns into two broad categories. In the first, genes were expressed in neurons underlying the VZ (Figures 7D–7F″; Figures S6D–S6F) (some of them only regionally; e.g., Figures 7E–E″). These genes could reveal a maturation stage (ongoing or recent neurogenesis) or, alternatively, a specific neuronal identity(ies) born around the stage of analysis (2–3 mpf). Expression at 15 dpf and 1 mpf remained confined to a stripe underlying the VZ (not shown), arguing for the first interpretation. The second category included genes expressed in a scattered pattern across the depth of the pallial parenchyma, in some cases in specific pallial subdivisions (e.g., Dm or Dl) (Figures 7A–C″; Figures S6A–S6C). Expression of these genes therefore overlaps with multiple neuronal ages, suggesting that the corresponding identities are shared by neurons born across the fish lifespan. Finally, we carefully analyzed the Dc area to determine, based on the sequential stacking model, whether some of the neocortical identities of amniotes were exclusively attributed/maintained in adult zebrafish pallial neurons born during embryogenesis. For all the markers considered, however, Dc was devoid of expression (Figure 7; Figure S6G). Within the limit of the selected marker genes chosen, these data suggest that the attribution of neuronal identities in the zebrafish pallium does not follow a simple scheme based on neuronal age or clonal lineage. To add support to this conclusion, we finally considered neurons expressing the neurotransmitters glutamate and GABA. Adult pallia from *her4*$^{H2a\text{-}mCherry,9TB(5dpf)}$ larvae were jointly processed for mCherry immunocytochemistry and in situ hybridization of *vglut* or *gad* transcripts. In both cases, positive neurons distributed within the neuronal layer born at 5 dpf, but also deeper as well as more superficially (Figure S7), confirming a broad age range for the generation of neurons of these phenotypes from the pallial VZ.

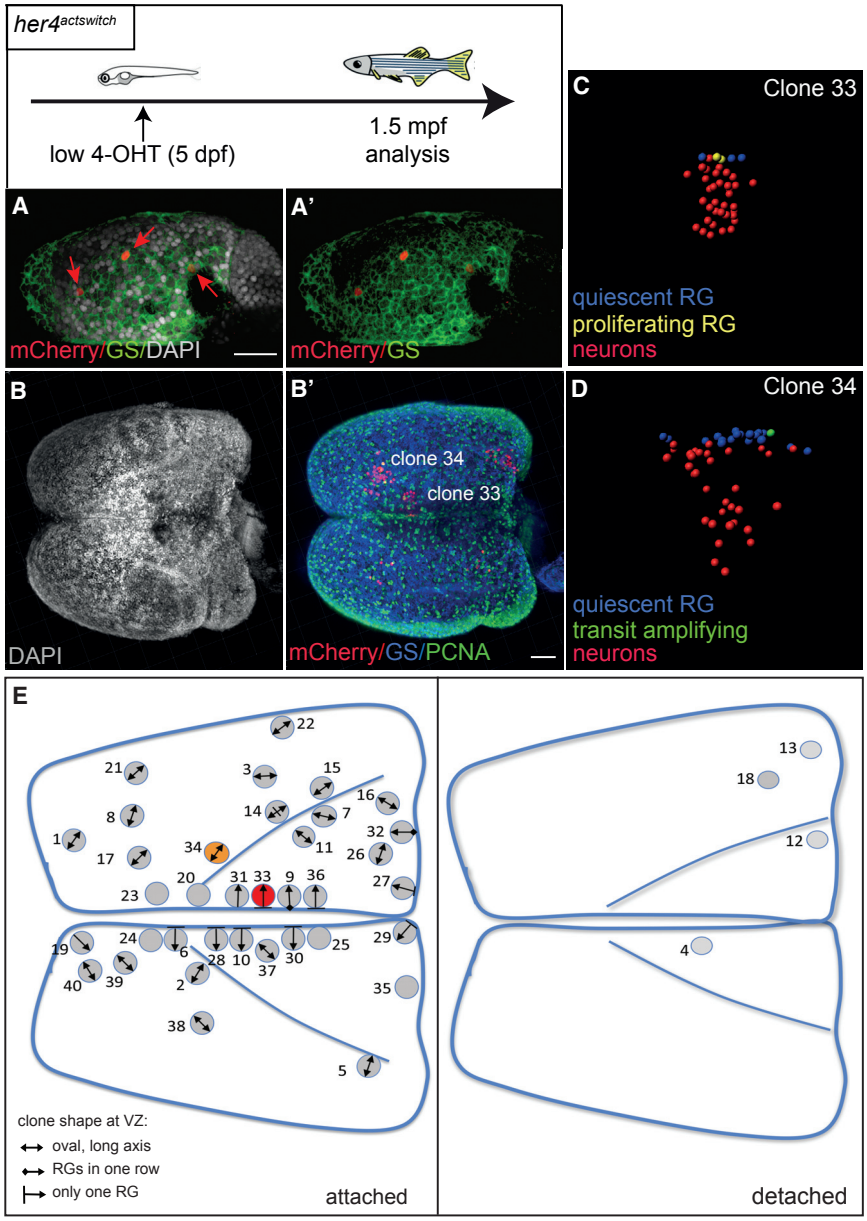

Figure 6. Clonal Analysis with Cell-Type Identification Confirms Long-Lasting Neurogenesis from Individual Pallial RGs

Top: experimental scheme.

(A and A′) Whole-mount dorsal view (anterior left) of a typical 6-dpf pallial hemisphere from a *her4*$^{actswitch,4OHT(5dpf)}$ fish stained at 1 day post-treatment for mCherry and GS (counterstained with DAPI). Red arrows point to individual recombined RGs.

(B and B′) Whole-mount dorsal view (anterior left) of a typical 1.5-mpf pallium from a *her4*$^{actswitch,4OHT(5dpf)}$ fish stained for mCherry, GS, and PCNA (B′).

(C and D) Segmented image of clone 33 (C) and clone 34 (D) highlighted in (B′) (color coded for cell types).

(E) Position of the 40 clones in flattened dorsal views of the 1.5-mpf pallium (clones 33 and 34 in B and B′ are colored). The shape of the VZ component of each clone is indicated (code bottom left).

See also Figure S5 and Table S3. Scale bars, 100 μm.

reward (Dm; similar to amygdalar nuclei), and cognitive tasks (Dm/Dl; resembling neocortical processing) [50–52]. Finally, Cre-mediated tracing demonstrated that these functional domains originate from the embryonic dorsal telencephalon, and their relative position fits their developmental origin when taking into account pallial eversion. These observations leave no doubt for the teleost pallium sharing developmental origin, neuroanatomical fields, and functions with that of tetrapods. From this starting point, we addressed here the key question of the pallial macroarchitecture and its generation from NSCs in zebrafish.

At the cell-population level, our results highlight the widespread and persistent neurogenic activity of zebrafish pallial RGs from embryonic stages until early adulthood (3 mpf), without major spatiotemporal gradients. A distinction should be made for the hippocampal area, where the generation of neurogenic RGs itself is delayed until early juvenile stages [21]. In all pallial territories, we failed to find evidence for major transit amplification, both from proliferation (this study) and clonal analyses [28], bringing the zebrafish pallial neurogenesis mode globally closer to that operating in amphibians, reptiles, and birds than mammals [10, 16, 47, 53–55]. Collectively, these species exhibit a net decrease in neurogenic output per NSC. The proportion of neurons per clone generated from pallial NSCs in gecko is lower than in mouse after 1 day [10]. Likewise, we find clones of 10–160 (on average 49) neurons per induced RG after 37 days (Table S3), compared to an average of 160 neurons per NSC in 11–20 days during neocortical neurogenesis in mouse [4].

DISCUSSION

Pallium Construction in Zebrafish Shares Distinct Traits with Mammalian and Non-mammalian Amniotes, Suggesting a Basal Pallial Layout

Developmental, hodological, functional, and lineage studies have unambiguously identified a pallial entity in jawed vertebrates, including teleosts. The dorsal telencephalons in mammals, birds, reptiles, amphibians, and teleosts share developmental markers [11, 12, 45–47], network, and functions at adult stage [48]. In teleosts, the preglomerular complex of the posterior tuberculum, a diencephalic nucleus relaying sensory modalities [49], is the primary source of ascending projections to a large Dm/Dl region, like the dorsal thalamus of tetrapods. The teleost pallium hosts functional fields processing spatial learning/memory (Dl; similar to the mammalian hippocampus),

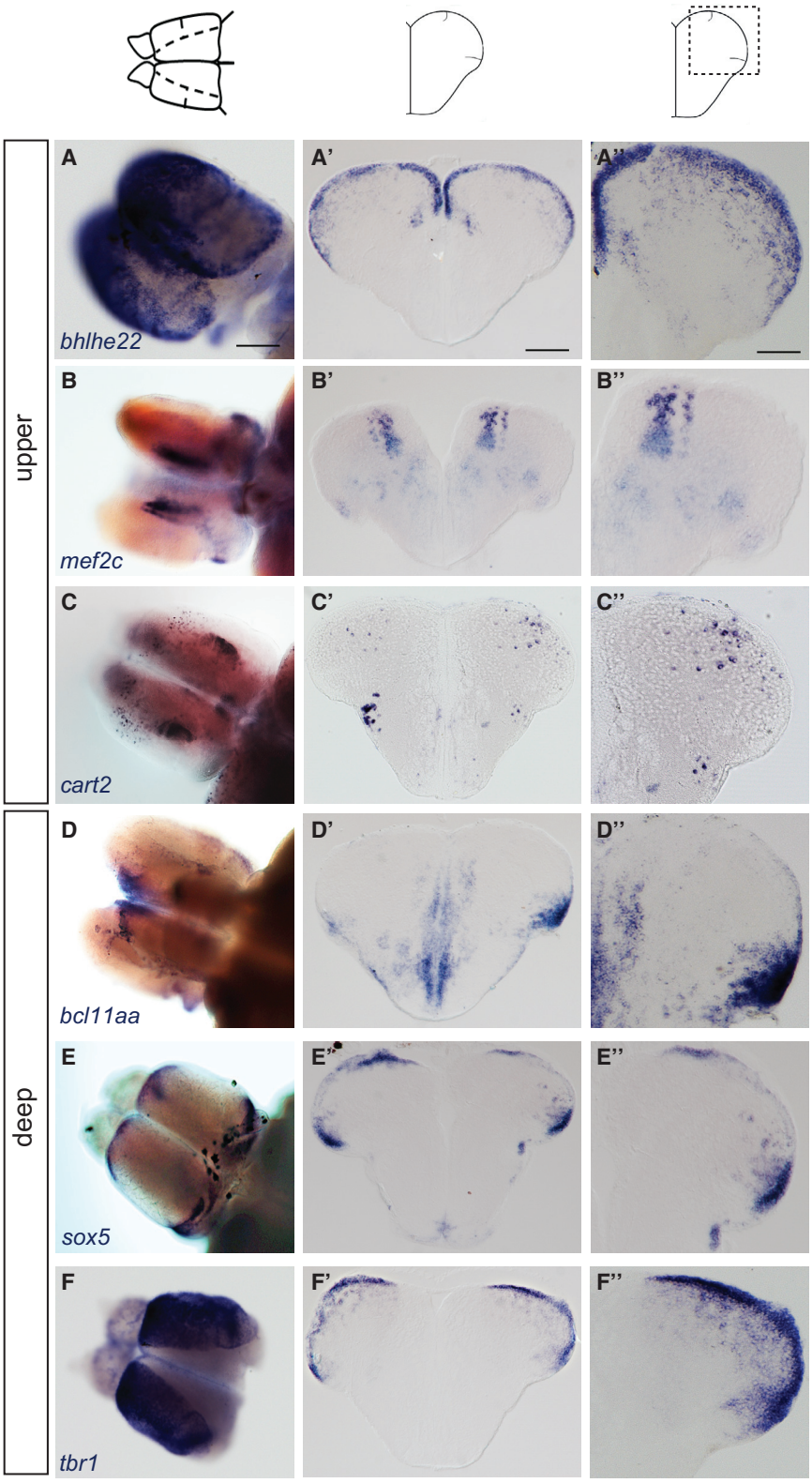

Figure 7. Expression in the Adult Zebrafish Pallium of Genes Identifying Neocortical Identities in Mammals and/or Birds

In situ hybridization of 2-mpf pallia (A–F: whole-mount views from the top; A′–F′: low and high magnifications of cross-sections at mid-antero-posterior levels, respectively) for 6 genes (Table S4) displaying scattered expression spanning age layers (A–C) or expression restricted to the neurogenic domain (D–F). Scale bars, 200 μm (A–F); 100 μm (A′–F′); and 50 μm (A′′–F′′). See also Figures S6 and S7.

Our work identifies for the first time the relationship between NSC activity and the spatiotemporal generation of the adult zebrafish pallial structure. By combining genetic birthdating and clonal analyses, we reached several important conclusions: (1) pallial neurons originating from pallial VZ RGs are organized in an outside-in age-related disposition (taking as a landmark neuronal distribution relative to the position of the VZ, a more stable reference than parenchymal orientation when comparing species with an everted pallium such as teleosts); (2) neuronal deposition expands in all directions over time from a deep central core generated during embryogenesis; (3) the spatial refinement of age-related layers and centrifugal lineage clones argue, respectively, against massive neuronal migrations along the radial and horizontal (parallel to the VZ surface) dimensions; and (4) neuronal deposition is largely driven by continuous neurogenic activity from individual pallial RGs. These results reveal a sequential stacking mode of pallium construction, where the spatiotemporal control of RG activity is an important mechanism of structure generation—although we cannot formally exclude the contribution of local neuronal migrations to the final architecture.

This simple strategy shares traits with neocortical organization in mammals, birds, and reptiles. Common denominators with mammals include the disposition of pallial VZ-derived neurons in age-related layers (although lamination is cryptic in zebrafish—only artificially revealed by our Tet-on induction time points—and mostly visible in neurons generated after early larval stages), the generation of clonally related neuronal "columns," and the neurogenic contribution of individual NSCs to all cortical layers. The latter point is particularly remarkable in zebrafish, where neurogenic RG activity extends over months. Columnar organization in mammals is proposed to reflect local functional circuitries [56]. We observed minimal inter-clone dispersion in the zebrafish pallium, also highlighting the existence of ontogenetic columns, the relevance of which needs to be studied. Finally, the inside-out disposition of excitatory neurons in the mammalian neocortex results from the radial outward migration of newborn neurons, notably following Reelin-dependent cues. The broad distribution of Reelin pathway components in the developing and adult zebrafish pallium may be non-permissive for oriented migration [57, 58].

The neocortex equivalent of other amniotes consists of a thin dorsal cortex ("Wulst" in birds) and an enlarged, laterally positioned "dorsal ventricular ridge" (DVR). The cortex shows layered arrangements in all phyla but very different cytoarchitectures: in birds, L4 and L5 neurons [15, 59, 60] support a vertical functional organization, which does not fully correspond to neuronal birthdates, as outside-in development is partially blurred by radial migrations [61]. In reptiles and turtles, the 3-layer cortex develops in an outside-in manner [16] but excitatory L4 and L5 neurons only position within layer 2, occupying different fields along the antero-posterior axis [15, 62, 63]. Finally, in all sauropsids studied, the DVR is organized in large nuclei of distinct L4 or L5 identities, at least in part corresponding to distinct birthdates [9, 15, 61]. Several mechanisms were postulated to account for generating these structures: the segregation of VZ territories concomitantly neurogenic but generating different neuronal fates in the reptilian cortex [15] and, in the bird DVR, the segregation of VZ territories with different neurogenic periods [9] or continuous VZ neurogenesis accompanied by neuronal migration and the coalescence of age-related neurons [61]. A precise comparison with the zebrafish pallium will obviously require knowledge of neuronal identities and/or analyses of connectivity. A common trait with non-mammalian amniotes is, however, the generation of outside-in age-related organizations and the most likely minimal contribution of neuronal migration events. Recently, cortical neuron generation was studied in the amphibian *Xenopus laevis* through larval stages and was also shown to display an outside-in organization [47], although the neurogenic activity of individual NPCs was not addressed.

In the absence of a fossil record of the brain, and because we are not working with ancestral species, evolutionary considerations should be made with caution. Our results first further highlight the amazing divergence in pallium construction modes of extant vertebrates, but also stress the apparent simplicity of pallial neurogenesis in the teleost zebrafish and indicate that it shares several traits with different amniote phyla. We propose that the spatiotemporal mode of zebrafish pallium construction may mimic a basal layout, from which the generation of amniote pallial structures could have diverged, with mammals evolving radial migration and layering and birds and reptiles applying regional constraints on NSC neurogenic activity. The fact that anamniote tetrapods such as *Xenopus* may use a structure generation process comparable to zebrafish [47] further supports this hypothesis.

Ontogeny of Presumed Neuroanatomical Domains in the Zebrafish Pallium

The cytoarchitectonic subdivisions of the zebrafish adult pallium [64] are based on the spatial organization of neuronal cell bodies within the adult parenchyma. In this regard, the present work is also important as it solves, with genetic arguments, long-standing and controversial issues on the significance of these subdivisions. We found that Dc is the sole territory matching a temporal ontogenetic window, its constituent neurons being all generated prior to 5 dpf—in a manner reminiscent of the deep domains of Dm, Dl, and Dp. We further show that Dc is generated from the VZ of Dm, Dl, and Da (Table S1). These results contradict the recent conclusion that Dc possesses its own germinative domain [33], and formally provide evidence for the hypothesis of Braford that Dc neurons do not reflect a primary pallial subdivision but correspond to the deep neurons of overlying subdivisions [65, 66]. In contrast to Dc, we find that neither Dm, Dl, nor Dp corresponds to defined temporal or clonal units.

Encoding Pallial Neuronal Identities

The chronological generation of different neuronal subtypes by pallial RGs is observed in all amniotes [9, 10, 15]. It is unknown, however, whether it extends to other vertebrates, and whether all neuronal subtypes are shared between species. Classical anatomical studies in teleosts suggest that superficial and deep (Dc) neurons are of different identities, with periventricular pallial zones composed of small stellate neurons with widely branching dendrites receiving ascending sensory input, whereas deep pallial territories host large efferent neurons receiving most input from the more superficial neurons and, in the case of Dc, projections to the optic tectum [67–69]. The

present work demonstrates that these different neuronal subtypes are generated at different stages, periventricular neurons being "young," whereas deep pallial neurons are "old." Thus, at the population level, the bulk of neuronal identities most likely vary over time during development to adulthood. Because we also show that individual RGs are capable of generating, sequentially, these old then young neuronal subtypes (Figure 5), our findings suggest that the sequential encoding of neuronal identities by pallial NSCs is a shared feature extending to teleosts.

A correlated question is how neuronal identities in the zebrafish adult pallium compare with those of amniotes. Neurogenesis being lifelong in zebrafish, it is difficult to hypothesize on the expected expression of mammalian identifiers of cortical layers in the zebrafish adult pallium. Moreover, only a few of these "identifiers" in fact share expression patterns among amniotes, and are maintained in the adult brain. For this reason, we largely relied on markers expressed in similar neocortical layers in adult mouse and human [44] (Table S4) or mouse and ferret [15]. Although a majority of markers were expressed in the zebrafish adult pallium, superimposing birthdates and clones failed to extract a simple rule based on age or lineage that could account for their expression profile: there was no link between a subventricular or deep expression in the zebrafish adult pallium and mammalian markers of upper versus deep layers, and none of the markers tested identified adult neurons generated at embryonic or early larval stages. This could either indicate transient expression or neuronal subtypes that are not found in zebrafish. In support of the first hypothesis, *cux1b*, *cux2a*, *satb2*, *sox5*, *bcl1aa* (*ctip1*), and *fezf2* were expressed in rather broad parenchymal domains of the 5-dpf pallium but either absent (*cux1b*, *cux2a*, *satb2*) or confined to the neurogenic zone (*sox5*, *bcl1aa*, *fezf2*) in the adult pallium (Table S4 and not shown). In addition, markers such as *mef2c* and *cart*, expressed across a broad neuronal age range in the zebrafish pallium, identify functions rather than identities in rodents [70, 71]. In support of the second hypothesis, we never found expression of *bcl1bb* (*ctip2*) or *ER81*, diagnostic markers of L5 neurons in amniotes, or of the conserved L4 marker *Ror*β in the zebrafish pallium at either stage. Projections from the preglomerular complex argue for the existence of neurons functionally equivalent to amniote L4 neurons. Their molecular identity will need to be precisely assessed.

STAR★METHODS

Detailed methods are provided in the online version of this paper and include the following:

- KEY RESOURCES TABLE
- CONTACT FOR REAGENT AND RESOURCE SHARING
- EXPERIMENTAL MODEL AND SUBJECT DETAILS
  - Zebrafish Lines
  - Fish maintenance and staging
  - Ethical approval
- METHOD DETAILS
  - 4OHT and 9TB treatments
  - Immunohistochemistry and In Situ Hybridization
  - Whole-mount brain clearing
  - Confocal microscopy, image acquisition and processing
  - Multiphoton microscopy and related image analysis
- QUANTIFICATION AND STATISTICAL ANALYSIS

SUPPLEMENTAL INFORMATION

Supplemental Information includes seven figures, four tables, and two movies and can be found with this article online at https://doi.org/10.1016/j.cub.2017.09.052.

AUTHOR CONTRIBUTIONS

G.F., L.D., V.C., and I.F. conducted all experiments; Table S4 and corresponding expression patterns were analyzed in collaboration with A.J.M. and C.H.; N.V. and E.B. conducted the segmentation and image analysis of Brainbow clones (Figure 5; Figure S5; Movies S1 and S2); N.D. provided expertise with whole-mount image generation and analyses with Imaris; M.C. generated the Tet-on fish DNA constructs; and S.B. maintained the fish necessary to this study. L.B.-C. and I.F. directed the work, analyzed the data, and wrote the manuscript.

ACKNOWLEDGMENTS

We thank members of the L.B.-C. laboratory for their critical input, W. Supatto for advice on image analysis, and M. O'Connell for critical proofreading. Work in the L.B.-C. laboratory was funded by the Agence Nationale de la Recherche (grant ANR-2012-BSV4-0004-01), Ecole des Neurosciences de Paris (ENP), European Research Council (AdG 322936), and Labex Revive. E.B.'s contribution was supported by Agence Nationale de la Recherche (contracts ANR-10-INBS-04 France BioImaging and ANR-11-EQPX-0029 Morphoscope2). G.F. was recipient of a fellowship from the Erasmus Programme. C.H. was supported by the Medical Research Council (G0901525) and European Union ZF-Health Programme.

Received: April 24, 2017
Revised: August 14, 2017
Accepted: September 25, 2017
Published: October 26, 2017

REFERENCES

1. Suzuki, I.K., and Hirata, T. (2013). Neocortical neurogenesis is not really "neo": a new evolutionary model derived from a comparative study of chick pallial development. Dev. Growth Differ. *55*, 173–187.
2. Dugas-Ford, J., and Ragsdale, C.W. (2015). Levels of homology and the problem of neocortex. Annu. Rev. Neurosci. *38*, 351–368.
3. Molnár, Z. (2011). Evolution of cerebral cortical development. Brain Behav. Evol. *78*, 94–107.
4. Gao, P., Postiglione, M.P., Krieger, T.G., Hernandez, L., Wang, C., Han, Z., Streicher, C., Papusheva, E., Insolera, R., Chugh, K., et al. (2014). Deterministic progenitor behavior and unitary production of neurons in the neocortex. Cell *159*, 775–788.
5. Franco, S.J., Gil-Sanz, C., Martinez-Garay, I., Espinosa, A., Harkins-Perry, S.R., Ramos, C., and Müller, U. (2012). Fate-restricted neural progenitors in the mammalian cerebral cortex. Science *337*, 746–749.
6. Alcamo, E.A., Chirivella, L., Dautzenberg, M., Dobreva, G., Fariñas, I., Grosschedl, R., and McConnell, S.K. (2008). Satb2 regulates callosal projection neuron identity in the developing cerebral cortex. Neuron *57*, 364–377.
7. Toma, K., and Hanashima, C. (2015). Switching modes in corticogenesis: mechanisms of neuronal subtype transitions and integration in the cerebral cortex. Front. Neurosci. *9*, 274.
8. Noctor, S.C., Martinez-Cerdeño, V., and Kriegstein, A.R. (2007). Neural stem and progenitor cells in cortical development. Novartis Found. Symp. *288*, 59–73.

9. Suzuki, I.K., Kawasaki, T., Gojobori, T., and Hirata, T. (2012). The temporal sequence of the mammalian neocortical neurogenetic program drives mediolateral pattern in the chick pallium. Dev. Cell *22*, 863–870.
10. Nomura, T., Gotoh, H., and Ono, K. (2013). Changes in the regulation of cortical neurogenesis contribute to encephalization during amniote brain evolution. Nat. Commun. *4*, 2206.
11. Fernandez, A.S., Pieau, C., Repérant, J., Boncinelli, E., and Wassef, M. (1998). Expression of the Emx-1 and Dlx-1 homeobox genes define three molecularly distinct domains in the telencephalon of mouse, chick, turtle and frog embryos: implications for the evolution of telencephalic subdivisions in amniotes. Development *125*, 2099–2111.
12. Puelles, L., Kuwana, E., Puelles, E., Bulfone, A., Shimamura, K., Keleher, J., Smiga, S., and Rubenstein, J.L.R. (2000). Pallial and subpallial derivatives in the embryonic chick and mouse telencephalon, traced by the expression of the genes Dlx-2, Emx-1, Nkx-2.1, Pax-6, and Tbr-1. J. Comp. Neurol. *424*, 409–438.
13. Csillag, A. (1999). Striato-telencephalic and striato-tegmental circuits: relevance to learning in domestic chicks. Behav. Brain Res. *98*, 227–236.
14. Zeier, H., and Karten, H.J. (1971). The archistriatum of the pigeon: organization of afferent and efferent connections. Brain Res. *31*, 313–326.
15. Dugas-Ford, J., Rowell, J.J., and Ragsdale, C.W. (2012). Cell-type homologies and the origins of the neocortex. Proc. Natl. Acad. Sci. USA *109*, 16974–16979.
16. Goffinet, A.M., Daumerie, C., Langerwerf, B., and Pieau, C. (1986). Neurogenesis in reptilian cortical structures: ^{3}H-thymidine autoradiographic analysis. J. Comp. Neurol. *243*, 106–116.
17. Folgueira, M., Bayley, P., Navratilova, P., Becker, T.S., Wilson, S.W., and Clarke, J.D.W. (2012). Morphogenesis underlying the development of the everted teleost telencephalon. Neural Dev. *7*, 32.
18. Chapouton, P., Skupien, P., Hesl, B., Coolen, M., Moore, J.C., Madelaine, R., Kremmer, E., Faus-Kessler, T., Blader, P., Lawson, N.D., and Bally-Cuif, L. (2010). Notch activity levels control the balance between quiescence and recruitment of adult neural stem cells. J. Neurosci. *30*, 7961–7974.
19. Grupp, L., Wolburg, H., and Mack, A.F. (2010). Astroglial structures in the zebrafish brain. J. Comp. Neurol. *518*, 4277–4287.
20. Ganz, J., Kroehne, V., Freudenreich, D., Machate, A., Geffarth, M., Braasch, I., Kaslin, J., and Brand, M. (2014). Subdivisions of the adult zebrafish pallium based on molecular marker analysis. F1000Res. *3*, 308.
21. Dirian, L., Galant, S., Coolen, M., Chen, W., Bedu, S., Houart, C., Bally-Cuif, L., and Foucher, I. (2014). Spatial regionalization and heterochrony in the formation of adult pallial neural stem cells. Dev. Cell *30*, 123–136.
22. Lim, D.A., and Alvarez-Buylla, A. (2014). Adult neural stem cells stake their ground. Trends Neurosci. *37*, 563–571.
23. Urbán, N., and Guillemot, F. (2014). Neurogenesis in the embryonic and adult brain: same regulators, different roles. Front. Cell. Neurosci. *8*, 396.
24. Götz, M., Nakafuku, M., and Petrik, D. (2016). Neurogenesis in the developing and adult brain—similarities and key differences. Cold Spring Harb. Perspect. Biol. *8*, a018853.
25. Yeo, S.Y., Kim, M., Kim, H.S., Huh, T.L., and Chitnis, A.B. (2007). Fluorescent protein expression driven by her4 regulatory elements reveals the spatiotemporal pattern of Notch signaling in the nervous system of zebrafish embryos. Dev. Biol. *301*, 555–567.
26. Cheung, A.F.P., Pollen, A.A., Tavare, A., DeProto, J., and Molnár, Z. (2007). Comparative aspects of cortical neurogenesis in vertebrates. J. Anat. *211*, 164–176.
27. Charvet, C.J., Owerkowicz, T., and Striedter, G.F. (2009). Phylogeny of the telencephalic subventricular zone in sauropsids: evidence for the sequential evolution of pallial and subpallial subventricular zones. Brain Behav. Evol. *73*, 285–294.
28. Rothenaigner, I., Krecsmarik, M., Hayes, J.A., Bahn, B., Lepier, A., Fortin, G., Götz, M., Jagasia, R., and Bally-Cuif, L. (2011). Clonal analysis by distinct viral vectors identifies bona fide neural stem cells in the adult zebrafish telencephalon and characterizes their division properties and fate. Development *138*, 1459–1469.
29. Qiu, J., Papatsenko, D., Niu, X., Schaniel, C., and Moore, K. (2014). Divisional history and hematopoietic stem cell function during homeostasis. Stem Cell Reports *2*, 473–490.
30. Furutachi, S., Miya, H., Watanabe, T., Kawai, H., Yamasaki, N., Harada, Y., Imayoshi, I., Nelson, M., Nakayama, K.I., Hirabayashi, Y., and Gotoh, Y. (2015). Slowly dividing neural progenitors are an embryonic origin of adult neural stem cells. Nat. Neurosci. *18*, 657–665.
31. Campbell, L.J., Willoughby, J.J., and Jensen, A.M. (2012). Two types of Tet-On transgenic lines for doxycycline-inducible gene expression in zebrafish rod photoreceptors and a Gateway-based Tet-On toolkit. PLoS ONE *7*, e51270.
32. Halterman, M.W. (2011). An improved method for the study of apoptosis-related genes using the Tet-On system. J. Biomol. Screen. *16*, 332–337.
33. Mueller, T., Dong, Z., Berberoglu, M.A., and Guo, S. (2011). The dorsal pallium in zebrafish, *Danio rerio* (Cyprinidae, Teleostei). Brain Res. *1381*, 95–105.
34. Boniface, E.J., Lu, J., Victoroff, T., Zhu, M., and Chen, W. (2009). FlEx-based transgenic reporter lines for visualization of Cre and Flp activity in live zebrafish. Genesis *47*, 484–491.
35. Mosimann, C., Kaufman, C.K., Li, P., Pugach, E.K., Tamplin, O.J., and Zon, L.I. (2011). Ubiquitous transgene expression and Cre-based recombination driven by the ubiquitin promoter in zebrafish. Development *138*, 169–177.
36. Pan, Y.A., Livet, J., Sanes, J.R., Lichtman, J.W., and Schier, A.F. (2011). Multicolor Brainbow imaging in zebrafish. Cold Spring Harb. Protoc. *2011*, pdb.prot5546.
37. Pan, Y.A., Freundlich, T., Weissman, T.A., Schoppik, D., Wang, X.C., Zimmerman, S., Ciruna, B., Sanes, J.R., Lichtman, J.W., and Schier, A.F. (2013). Zebrabow: multispectral cell labeling for cell tracing and lineage analysis in zebrafish. Development *140*, 2835–2846.
38. Wang, Y., Rovira, M., Yusuff, S., and Parsons, M.J. (2011). Genetic inducible fate mapping in larval zebrafish reveals origins of adult insulin-producing β-cells. Development *138*, 609–617.
39. Alunni, A., Krecsmarik, M., Bosco, A., Galant, S., Pan, L., Moens, C.B., and Bally-Cuif, L. (2013). Notch3 signaling gates cell cycle entry and limits neural stem cell amplification in the adult pallium. Development *140*, 3335–3347.
40. Guillemot, F., Molnár, Z., Tarabykin, V., and Stoykova, A. (2006). Molecular mechanisms of cortical differentiation. Eur. J. Neurosci. *23*, 857–868.
41. Arlotta, P., Molyneaux, B.J., Chen, J., Inoue, J., Kominami, R., and Macklis, J.D. (2005). Neuronal subtype-specific genes that control corticospinal motor neuron development in vivo. Neuron *45*, 207–221.
42. Cobos, I., and Seeley, W.W. (2015). Human von Economo neurons express transcription factors associated with layer V subcerebral projection neurons. Cereb. Cortex *25*, 213–220.
43. Leifer, D., Li, Y.L., and Wehr, K. (1997). Myocyte-specific enhancer binding factor 2C expression in fetal mouse brain development. J. Mol. Neurosci. *8*, 131–143.
44. Molyneaux, B.J., Arlotta, P., Menezes, J.R.L., and Macklis, J.D. (2007). Neuronal subtype specification in the cerebral cortex. Nat. Rev. Neurosci. *8*, 427–437.
45. Mueller, T., Wullimann, M.F., and Guo, S. (2008). Early teleostean basal ganglia development visualized by zebrafish Dlx2a, Lhx6, Lhx7, Tbr2 (eomesa), and GAD67 gene expression. J. Comp. Neurol. *507*, 1245–1257.
46. Wullimann, M.F., and Mueller, T. (2004). Teleostean and mammalian forebrains contrasted: evidence from genes to behavior. J. Comp. Neurol. *475*, 143–162.
47. Moreno, N., and González, A. (2017). Pattern of neurogenesis and identification of neuronal progenitor subtypes during pallial development in *Xenopus laevis*. Front. Neuroanat. *11*, 24.
48. Karten, H.J. (2013). Neocortical evolution: neuronal circuits arise independently of lamination. Curr. Biol. *23*, R12–R15.

49. Northcutt, R.G. (2008). Forebrain evolution in bony fishes. Brain Res. Bull. *75*, 191–205.
50. von Trotha, J.W., Vernier, P., and Bally-Cuif, L. (2014). Emotions and motivated behavior converge on an amygdala-like structure in the zebrafish. Eur. J. Neurosci. *40*, 3302–3315.
51. Portavella, M., Torres, B., and Salas, C. (2004). Avoidance response in goldfish: emotional and temporal involvement of medial and lateral telencephalic pallium. J. Neurosci. *24*, 2335–2342.
52. Portavella, M., Vargas, J.P., Torres, B., and Salas, C. (2002). The effects of telencephalic pallial lesions on spatial, temporal, and emotional learning in goldfish. Brain Res. Bull. *57*, 397–399.
53. Nomura, T., Takahashi, M., Hara, Y., and Osumi, N. (2008). Patterns of neurogenesis and amplitude of Reelin expression are essential for making a mammalian-type cortex. PLoS ONE *3*, e1454.
54. Nomura, T., Ohtaka-Maruyama, C., Yamashita, W., Wakamatsu, Y., Murakami, Y., Calegari, F., Suzuki, K., Gotoh, H., and Ono, K. (2016). The evolution of basal progenitors in the developing non-mammalian brain. Development *143*, 66–74.
55. Taverna, E., Götz, M., and Huttner, W.B. (2014). The cell biology of neurogenesis: toward an understanding of the development and evolution of the neocortex. Annu. Rev. Cell Dev. Biol. *30*, 465–502.
56. Rakic, P. (1988). Specification of cerebral cortical areas. Science *241*, 170–176.
57. Costagli, A., Kapsimali, M., Wilson, S.W., and Mione, M. (2002). Conserved and divergent patterns of Reelin expression in the zebrafish central nervous system. J. Comp. Neurol. *450*, 73–93.
58. Imai, H., Oomiya, Y., Kikkawa, S., Shoji, W., Hibi, M., Terashima, T., and Katsuyama, Y. (2012). Dynamic changes in the gene expression of zebrafish Reelin receptors during embryogenesis and hatching period. Dev. Growth Differ. *54*, 253–263.
59. Shimizu, T., Cox, K., and Karten, H.J. (1995). Intratelencephalic projections of the visual wulst in pigeons (*Columba livia*). J. Comp. Neurol. *359*, 551–572.
60. Wild, J.M., and Williams, M.N. (2000). Rostral wulst in passerine birds. I. Origin, course, and terminations of an avian pyramidal tract. J. Comp. Neurol. *416*, 429–450.
61. Striedter, G.F., and Keefer, B.P. (2000). Cell migration and aggregation in the developing telencephalon: pulse-labeling chick embryos with bromodeoxyuridine. J. Neurosci. *20*, 8021–8030.
62. Ulinski, P. (1990). The cerebral cortex of reptiles. In Cerebral Cortex, E. Jones, and A. Peters, eds. (Plenum), pp. 139–216.
63. Connors, B.W., and Kriegstein, A.R. (1986). Cellular physiology of the turtle visual cortex: distinctive properties of pyramidal and stellate neurons. J. Neurosci. *6*, 164–177.
64. Wullimann, M.F., Rupp, B., and Reichert, H. (1996). Neuroanatomy of the Zebrafish Brain: A Topological Atlas (Birkhäuser).
65. Nieuwenhuys, R. (1963). The comparative anatomy of the actinopterygian forebrain. J. Hirnforsch. *7*, 171–192.
66. Braford, M.R., Jr. (1995). Comparative aspects of forebrain organization in the ray-finned fishes: touchstones or not? Brain Behav. Evol. *46*, 259–274.
67. Demski, L., and Beaver, J. (2001). Brain and cognitive function in teleost fishes. In Brain Evolution and Cognition, G. Roth, and M. Wullimann, eds. (Wiley), pp. 297–332.
68. Northcutt, R.G. (2006). Connections of the lateral and medial divisions of the goldfish telencephalic pallium. J. Comp. Neurol. *494*, 903–943.
69. Northcutt, R.G. (2011). Do teleost fishes possess a homolog of mammalian isocortex? Brain Behav. Evol. *78*, 136–138.
70. Harrington, A.J., Raissi, A., Rajkovich, K., Berto, S., Kumar, J., Molinaro, G., Raduazzo, J., Guo, Y., Loerwald, K., Konopka, G., et al. (2016). MEF2C regulates cortical inhibitory and excitatory synapses and behaviors relevant to neurodevelopmental disorders. eLife *5*, e20059.
71. Subhedar, N.K., Nakhate, K.T., Upadhya, M.A., and Kokare, D.M. (2014). CART in the brain of vertebrates: circuits, functions and evolution. Peptides *54*, 108–130.
72. Kwan, K.M., Fujimoto, E., Grabher, C., Mangum, B.D., Hardy, M.E., Campbell, D.S., Parant, J.M., Yost, H.J., Kanki, J.P., and Chien, C.B. (2007). The Tol2kit: a multisite Gateway-based construction kit for Tol2 transposon transgenesis constructs. Dev. Dyn. *236*, 3088–3099.
73. Bernardos, R.L., and Raymond, P.A. (2006). GFAP transgenic zebrafish. Gene Expr. Patterns *6*, 1007–1013.
74. Kimmel, C.B., Ballard, W.W., Kimmel, S.R., Ullmann, B., and Schilling, T.F. (1995). Stages of embryonic development of the zebrafish. Dev. Dyn. *203*, 253–310.
75. Bosco, A., Bureau, C., Affaticati, P., Gaspar, P., Bally-Cuif, L., and Lillesaar, C. (2013). Development of hypothalamic serotoninergic neurons requires Fgf signalling via the ETS-domain transcription factor Etv5b. Development *140*, 372–384.
76. Higashijima, S., Mandel, G., and Fetcho, J.R. (2004). Distribution of prospective glutamatergic, glycinergic, and GABAergic neurons in embryonic and larval zebrafish. J. Comp. Neurol. *480*, 1–18.
77. Hama, H., Kurokawa, H., Kawano, H., Ando, R., Shimogori, T., Noda, H., Fukami, K., Sakaue-Sawano, A., and Miyawaki, A. (2011). Scale: a chemical approach for fluorescence imaging and reconstruction of transparent mouse brain. Nat. Neurosci. *14*, 1481–1488.
78. Susaki, E.A., Tainaka, K., Perrin, D., Yukinaga, H., Kuno, A., and Ueda, H.R. (2015). Advanced CUBIC protocols for whole-brain and whole-body clearing and imaging. Nat. Protoc. *10*, 1709–1727.
79. Mahou, P., Zimmerley, M., Loulier, K., Matho, K.S., Labroille, G., Morin, X., Supatto, W., Livet, J., Débarre, D., and Beaurepaire, E. (2012). Multicolor two-photon tissue imaging by wavelength mixing. Nat. Methods *9*, 815–818.
80. Preibisch, S., Saalfeld, S., and Tomancak, P. (2009). Globally optimal stitching of tiled 3D microscopic image acquisitions. Bioinformatics *25*, 1463–1465.

STAR★METHODS

KEY RESOURCES TABLE

REAGENT or RESOURCE	SOURCE	IDENTIFIER
Antibodies		
Rabbit polyclonal anti-mCherry 1/300	Clontech	Cat#632496; RRID: AB_10013483
Chicken polyclonal anti-GFP 1/1000	Aves lab	Cat#GFP-1020; RRID: AB_10000240
Mouse monoclonal (IgG2a) anti-PCNA	Santa Cruz	Cat# sc-56 AB-16.0387; RRID: AB_628110
Rabbit polyclonal (IgG2a) anti-PCNA 1/500	GeneTex	Cat#GTX124496 AB-16.0386; RRID: AB_11161916
Mouse monoclonal (IgG1) anti-Flag 1/500	Sigma	Cat#F1804 AB-16.0331; RRID: AB_262044
Mouse monoclonal (IgG2a) anti-GS 1/1000Clone GS-6	Millipore	Cat#MAB302 AB-16.0342
Human polyclonal anti-Hu 1/10000	Gift from B. Zalk	AB-16.0356
Anti-Parvalbumine 1/2000	Millipore	Cat#MAB1572 AB-16.0382
Chemicals, Peptides, and Recombinant Proteins		
4-Hydroxytamoxifen	Sigma-Aldrich	T176; CAS: 68392-35-8
9-tert-ButylDoxycycline, hydrocloride salt	Echelon Biosciences	B-0801; CAS: 233585-94-9
DAPI	Sigma-Aldrich	D9542; CAS: 28718-90-3
Critical Commercial Assays		
Taq DNA polymerase	EmeraldAmp Takara	Cat# 330A
Experimental Models: Organisms/Strains		
Zebrafish: Tg(*T2Kβactin:lox-stop-lox-hmgb1-mcherry*)^{ih15}	[38]	ZFIN ID: ZDB-TGCONSTRCT-110221-4
Zebrafish: Tg(*her4.1:EGFP*)^{y83}	[25]	ZFIN ID: ZDB-FISH-150901-14830
Zebrafish: *Tg(−3her4.3:ERT2-Cre-ERT2)*^{vu298a}	[33]	N/A
Zebrafish: Tg(*-3.5ubi:loxP-GFP-loxP-mCherry*)	[72]	ZFIN ID: ZDB-ALT-070612-3
Zebrafish: Tg(*ubb:LOX2272-LOXP-RFP-LOX2272-CFP-LOXP-YFP*)^{a131}, *ubi:Zebrabow-M*	[73]	ZFIN ID: ZDB-ALT-110825-11
Zebrafish: Tg(*her4:rtTA, cmlc2:GFP)*	[71]	ZFIN ID: ZDB-PUB-101209-26
Zebrafish: Tg(*GFP:biTRE:H2amCherry,crist:Venus)*	[36]	ZFIN ID: ZDB-ALT-130816-2
Oligonucleotides		
rtTA probe fw: ATGTCTAGACTGGACAAGAGCAAAGTC, rv:GGA TCCATTAACCCTCACTAAAGGGACTAACTGTCGACCTTGTC.	N/A	N/A
her4AttB4-fw: GGGGACAACTTTGTATAGAAAAGTTGTTTTGCAT TATTTCCCTAATTTTAAATGTC (−999-1028bp from AY691485.1) her4AttB1-Rv: GGGGACTGCTTTTTTGTACAAACTTGGTCA GGATCAGATCTGAGCTG (−3389-3409bp from AY691485.1)	N/A	N/A
Recombinant DNA		
her4:rtTA,GFP:cmlc2	This paper	N/A
GFP:biTRE:H2amCherry,crist:Venus	This paper	N/A
tetOn Toolkit	[31]	https://www.bio.umass.edu/biology/jensen/node/5
Tol2kit	[72]	http://tol2kit.genetics.utah.edu/index.php/Main_Page
Software and Algorithms		
Imaris (Spot Segmentation)	Bitplane	http://www.bitplane.com/imaris/imaris
Photoshop CS6	N/A	N/A
ZEN Black software	Carl Zeiss, Germany	https://www.zeiss.fr/microscopie/produits/microscope-software/zen.html
MATLAB 2014b, 2015b (Data analysis)	MathWorks	http://www.mathworks.com

CONTACT FOR REAGENT AND RESOURCE SHARING

Further information and requests for resources and reagents should be directed to and will be fulfilled by the Lead Contact, Laure Bally-Cuif (laure.bally-cuif@pasteur.fr). Sharing of zebrafish lines and constructs are subject to MTA request from Institut Pasteur.

EXPERIMENTAL MODEL AND SUBJECT DETAILS

Zebrafish Lines

The *her4:rtTA, GFP:cmlc2* and the *GFP:biTRE:H2amCherry, crist:Venus* constructs were obtained with the gateway strategy and the TetOn Toolkit [31]. The *her4.1* regulatory region was amplified as a 2411bp fragment by PCR using AB wild-type fish genomic DNA as template, followed by a BP reaction with pDONR P4-P1R (Tol2 kit) [72]. The *Tg(her4:rtTA, GFP:cmlc2)* and the *Tg(GFP:biTRE:H2amCherry, crist:Venus)* transgenic lines were made by injecting 1-cell embryos with a mix containing 15ng/μL of plasmid and 15ng/μL of *transposase* capped RNA.

Fish maintenance and staging

Embryos/larvae up to 5dpf were maintained and staged as described [74]. Juvenile fish were staged by size as described in [21]. Adult zebrafish (3-6-month old) were maintained using standard fish husbandry protocols. Animals of both sexes were used indiscriminately.

Ethical approval

All experiments were carried out in accordance with the official regulatory standards of the Department of Essonne (agreement number A 91-577 to L.B.-C.) and Department of Paris (agreement number B75-15-22 to L.B.-C.).

METHOD DETAILS

4OHT and 9TB treatments

4OHT treatments were performed as described [35] (10so.: 5μM, 4 hr; 1 or 2 dpf: 5μM, 6 hr; 5 dpf: 5μM, 30 hr; 1.5mpf: 5μM, 100 hr). Fish were then washed, transferred into fresh water, and grown as usual. For clonal analyses, 1dpf Tg(*her4:ERT2CreERT2;ubi:zebrabow)* embryos were recombined for 1 hr with 5μM 4OHT and 5dpf Tg(*her4:ERT2CreERT2;-3.5ubi:loxP-GFP-loxP-mCherry*) larvae for 10min with 0.5μM 4OHT. 9TB was dissolved in water at a final stock concentration of 5mg/mL, then diluted in embryo medium prior to use (≤2 dpf: 2.5μg/mL, 6 hr; 5 dpf – 15 dpf: 10μg/mL, 6 hr; 1.5 mpf: 10μg/mL, 96 hr). 9TB treatments were performed in the dark at 28°C. In the *Tg(GFP:biTRE:H2amCherry, crist:Venus)* line, a small GFP cluster was visible in the parenchyma at posterior levels even in the absence of treatment (not shown); it did not interfere with our analysis. For polyclones analysis, 9TB was applied at 0.5μg/mL for 10min onto 1dpf embryos. The embryos were then rinsed, grown and analyzed at 5dpf. Control experiments to assess clonality were analyzed on embryos treated with 0.5μM 4OHT for 10min at 5dpf, followed by a one- to two-day chase (for mCherry to be visible). Nearest neighbor distances were calculated per hemisphere (Imaris spot to spot closest distance on 20 larval hemispheres) and their cumulative probability distribution was plotted. We chose induction conductions such that in more than 85% of cases, induced cells were distant from each other of more than 15μm (equivalent to 4 cells diameters). Our brainbow analysis indicates very few cases, if any, of clone fragmentations. We therefore estimated that an initial distance of 4-cell diameters in the majority of cases should be sufficient to avoid this issue. To assess the occurrence of clone fusion, we also compared the estimated numbers of clones at time t+2days and at the analysis time point, 1.5mpf, and found that both were equivalent (Figure S5). Three hemispheres with ambiguous cases were discarded, and isolated mCherry cells, which were often observed, were not analyzed.

Immunohistochemistry and In Situ Hybridization

Immunohistochemistry and in situ *hybridization* were performed as described previously [18, 75]. The *gad* probes were a mix of *gad65/67a/67b*; the *vglut* probes were a mix of *vglut1/2.1/2.2*, as published in [76].

Whole-mount brain clearing

Whole zebrabow dissected adult brains were cleared using the SCALE approach [77] and mounted in glycerol 35%. Whole $her4^{H2a\text{-}mCherry,9TB(15dpf)}$ mCherry immunostained brains were cleared using the CUBIC approach [78] with the following incubations: CUBIC-1, 37°C, overnight; primary antibody, 37°C, 48 hr; secondary antibody, 37°C, 24 hr, CUBIC-2, overnight. Mounting was done in CUBIC-2.

Confocal microscopy, image acquisition and processing

All images except Figures 3E–3F′, 5, S5, S6, and 7 were taken using an inverted confocal microscope (Zeiss LSM700) and processed with the ZEN 2011 software (Carl Zeiss MicroImaging). Figures 2, 3A–3D, and S4A–S4L images are tile scans followed by maximum intensity projections of 8 squares and around 20 confocal optical sections. Images were then processed with Imaris or Photoshop CS6. Figures 3E–3F′, S7M, and S7N were processed with a median filter 3x3x3 followed or not by removal of object bigger than 250μm to remove background in the vessels or surface background. In situ *hybridization* pictures (Figure 7; Figure S6) were

photographed with a Zeiss Axiozoom V6 Macroscope. CUBIC cleared brain was imaged using an upright confocal microscope (Zeiss LSM710) with a Plan-Apochromat 20X/0,8 M27 objective.

Multiphoton microscopy and related image analysis

Large-volume multicolor two-photon microscopy was performed using the wavelength mixing method described in [79]. Imaging was performed on a lab-built multiphoton point-scanning microscope constructed around an inverted frame (IX-70, Olympus, Japan) and integrating galvo scanners (VM500+, GSI, USA), a high-index immersion objective with 4mm working distance (XLPN25XSVMP, Olympus) and a motorized sample stage for mosaic acquisition (PS3H122 and ProScan H117, Prior Scientific). Excitation was provided by a Titanium-sapphire oscillator (Chameleon Ultra2, Coherent, USA) and an optical parametric oscillator (compact OPO, Coherent, USA). For simultaneous excitation of CFP, YFP and RFP signals, TiS, OPO and two-color equivalent excitation $\lambda_3 = 2/(1/\lambda_{TiS} + 1/\lambda_{OPO})$ wavelengths were set to 850 nm, 1100 nm and 959 nm, respectively. Nonlinear signals were selected with appropriate dichroics (Semrock FF520-Di02 FF560-Di01) and filters (Semrock FF01-475/64 FF01-538/40 FF01-607/70), and epidetected on three separate channels by photomultiplier modules (P25PC SensTech UK and H7422P-40 Hamamatsu Japan) and lab-designed photon counting electronics. The pixel dwell time was 12 μs, and the voxel size was $0.8 \times 0.8 \times 2\ \mu m^3$. For whole pallium imaging, cleared brains were mounted on Scale media between two 150μm-thick glass coverslips separated by a spacer, and a mosaic of 9×6 volumes each encompassing $260 \times 285 \times 1000\ \mu m^3$ with a 20% lateral overlap was recorded.

Multicolor multiphoton stacks were preprocessed for flat-field correction and stitched with the open-source FIJI *Image Stitching* plugin using the *Max Intensity* fusion method [80]. Unlike cells, blood vessels exhibited intense fluorescence in all three channels and appeared ''white.'' These signals were removed using MATLAB by zeroing pixels having this characteristic. This processing step removed the vessels images without affecting cell signals. Semi-automatic cell detection was then performed using the Imaris Spot detection tool separately in the three channels. The automated detection exhibited an error rate (missed cells and false positives) of 50%–60%. Manual correction was then performed, which led to an uncertainty rate of 3%–5% for cell detection. Finally, clones were manually identified, based on cell colors, spatial clustering and cell sizes. The sparsity of labeling led to only a few ambiguous cases, which were discarded.

QUANTIFICATION AND STATISTICAL ANALYSIS

All details on the number of brains, hemispheres or cells processed can be found in the text and legends for figures (Figures S5E and S5F). n = 20 pallial hemispheres at 1dpt and 24 pallial hemispheres at 1.5mpt. The numbers in bracket indicate the number of hemispheres concerned for each number of induced cells/clones (Figure 5F). Data are presented as mean ± SEM, and statistical differences were determined using t test, $p < 0,25$. sem: 0.32 at 1dpt, 0.28 at 1.5mpt. For Figure S3B, n = 3 brains, t-test, non significant.

Current Biology, Volume *27*

Supplemental Information

Life-Long Neurogenic Activity of Individual Neural Stem Cells and Continuous Growth Establish an Outside-In Architecture in the Teleost Pallium

Giacomo Furlan, Valentina Cuccioli, Nelly Vuillemin, Lara Dirian, Anna Janue Muntasell, Marion Coolen, Nicolas Dray, Sébastien Bedu, Corinne Houart, Emmanuel Beaurepaire, Isabelle Foucher, and Laure Bally-Cuif

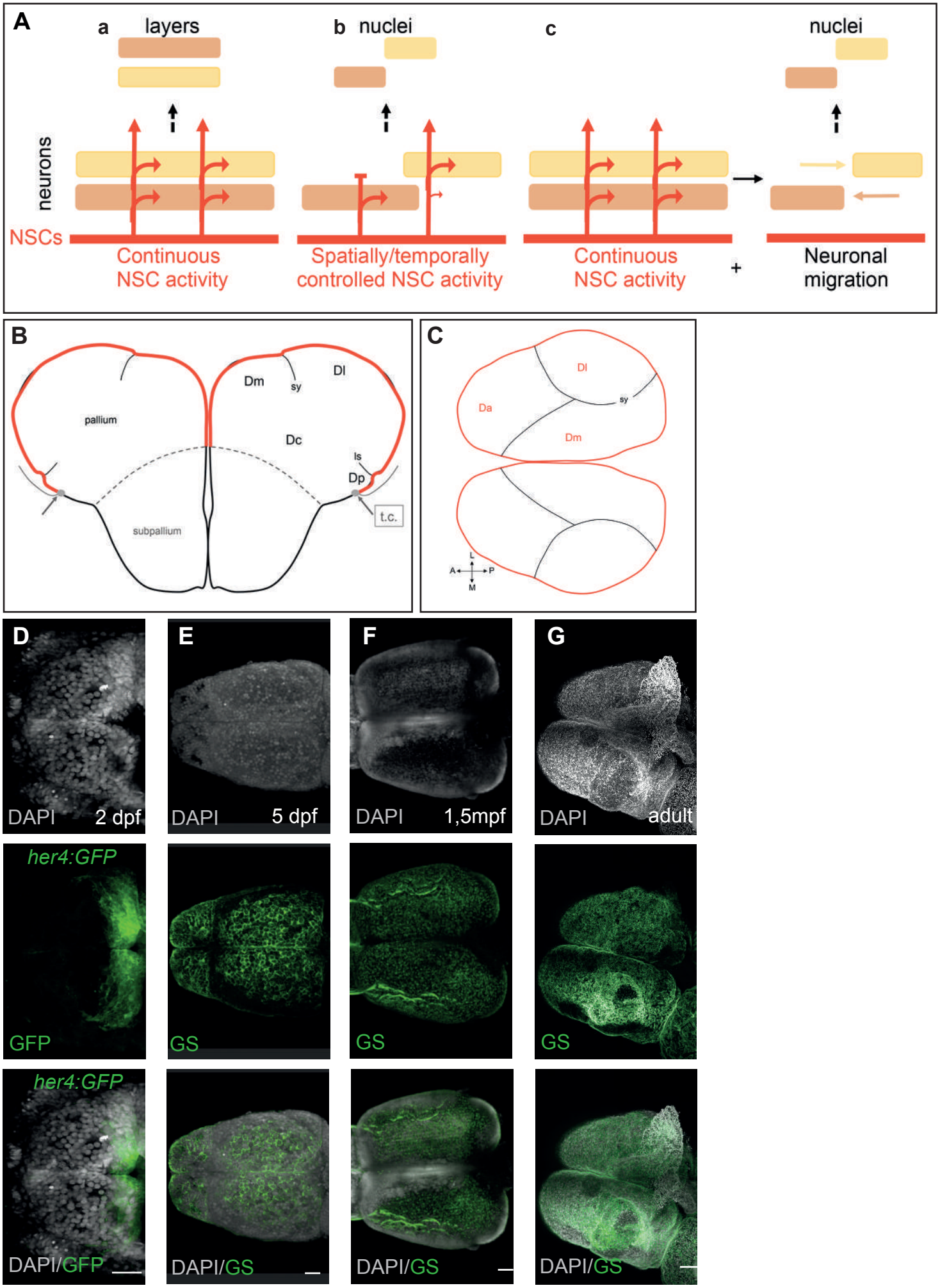
A
a layers
b nuclei
c
nuclei
neurons
NSCs
Continuous NSC activity
Spatially/temporally controlled NSC activity
Continuous NSC activity
+
Neuronal migration
B
pallium
Dm
sy
Dl
Dc
ls
Dp
t.c.
subpallium
C
Dl
Da
sy
Dm
L
A
P
M
D
DAPI
2 dpf
E
DAPI
5 dpf
F
DAPI
1,5mpf
G
DAPI
adult
her4:GFP
GFP
GS
GS
GS
her4:GFP
DAPI/GFP
DAPI/GS
DAPI/GS
DAPI/GS

Figure S1

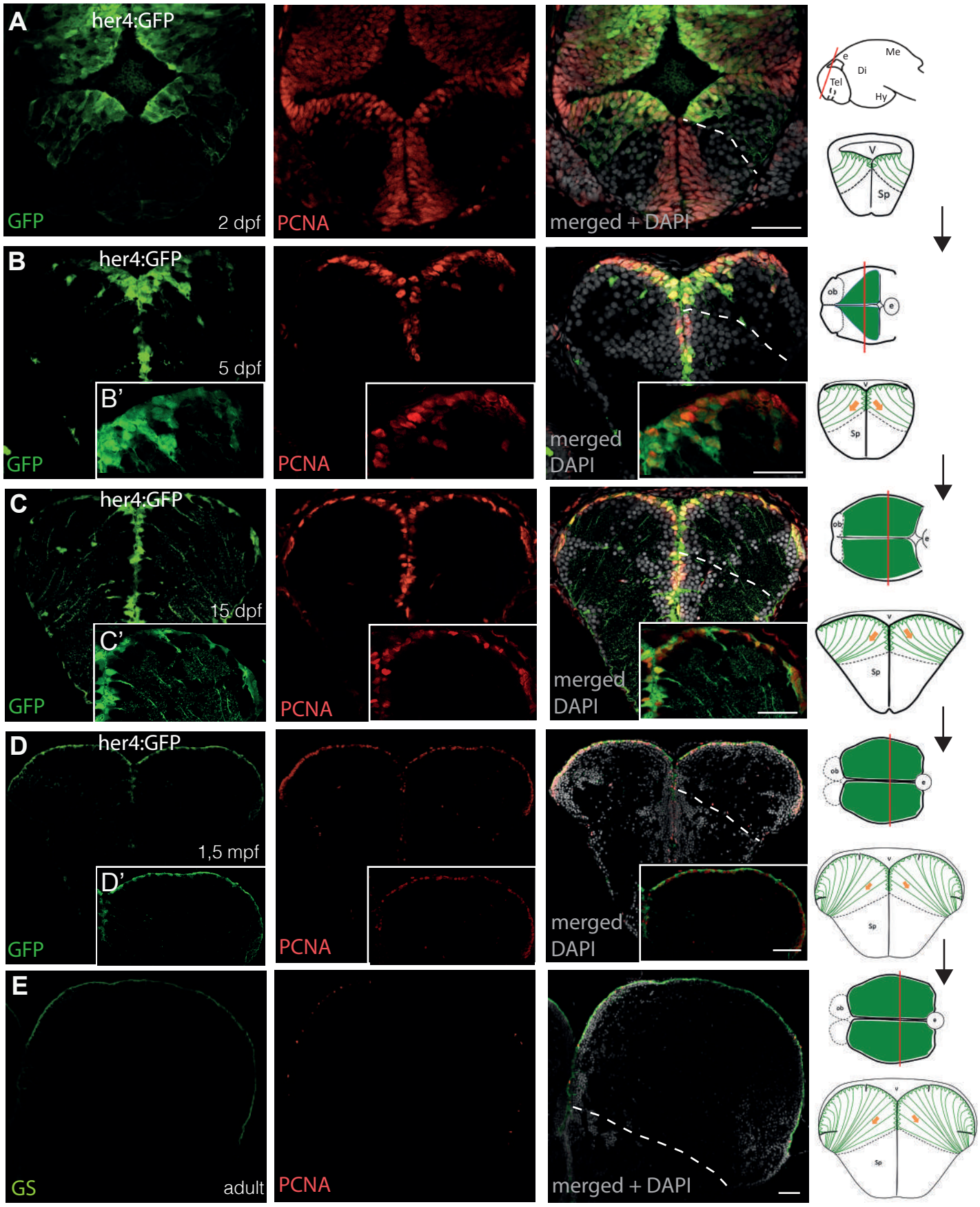
A
her4:GFP
GFP
2 dpf
PCNA
merged + DAPI
e
Me
Di
Tel
Hy
V
Sp
B
her4:GFP
5 dpf
B'
GFP
PCNA
merged
DAPI
ob
e
C
her4:GFP
15 dpf
C'
GFP
PCNA
merged
DAPI
D
her4:GFP
1,5 mpf
D'
GFP
PCNA
merged
DAPI
E
GS
adult
PCNA
merged + DAPI

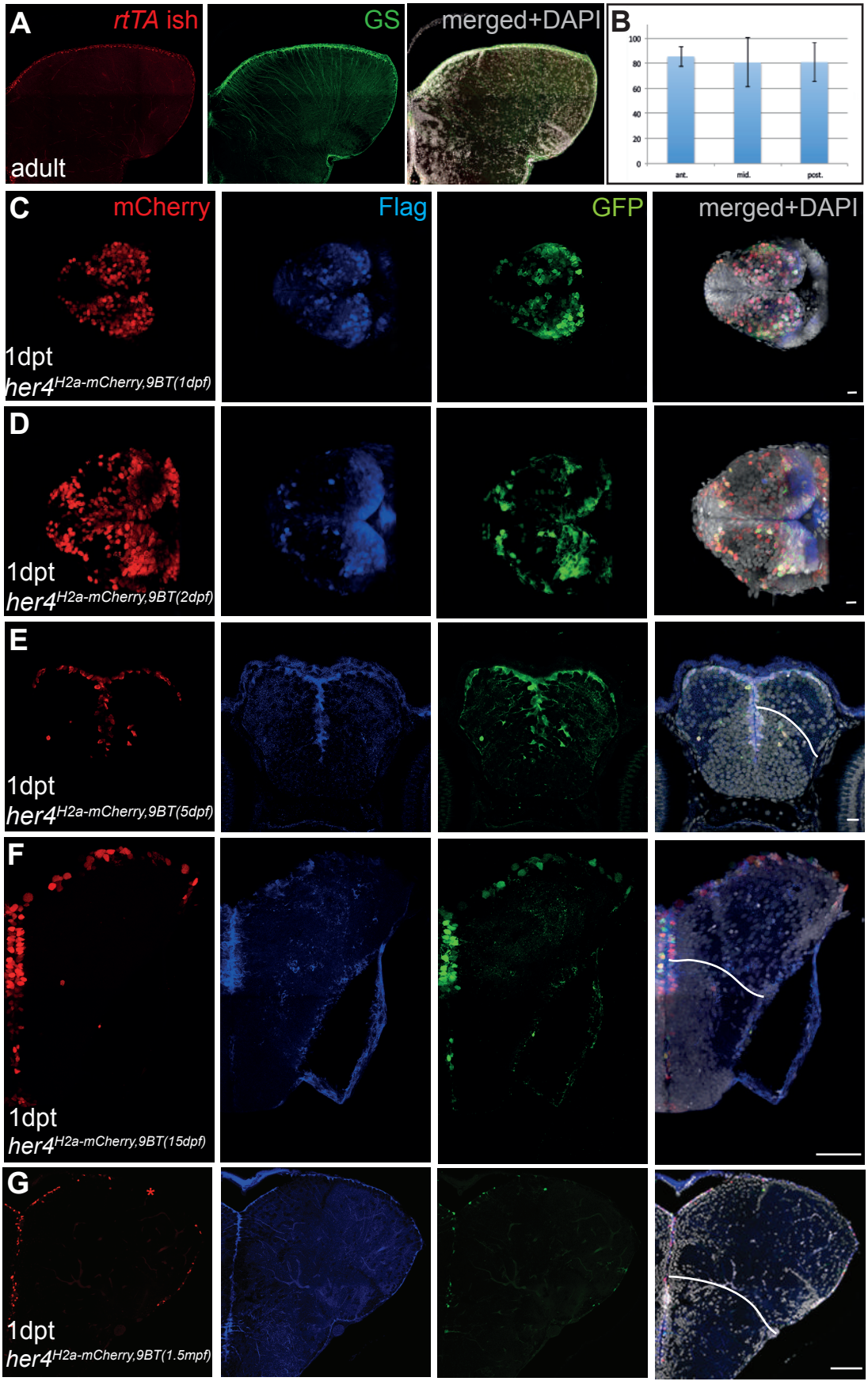
A
rtTA ish
adult
GS
merged+DAPI
B
100
80
60
40
20
0
ant.
mid.
post.
C
mCherry
Flag
GFP
merged+DAPI
1dpt
her4H2a-mCherry,9BT(1dpf)
D
1dpt
her4H2a-mCherry,9BT(2dpf)
E
1dpt
her4H2a-mCherry,9BT(5dpf)
F
1dpt
her4H2a-mCherry,9BT(15dpf)
G
1dpt
her4H2a-mCherry,9BT(1.5mpf)

Figure S3

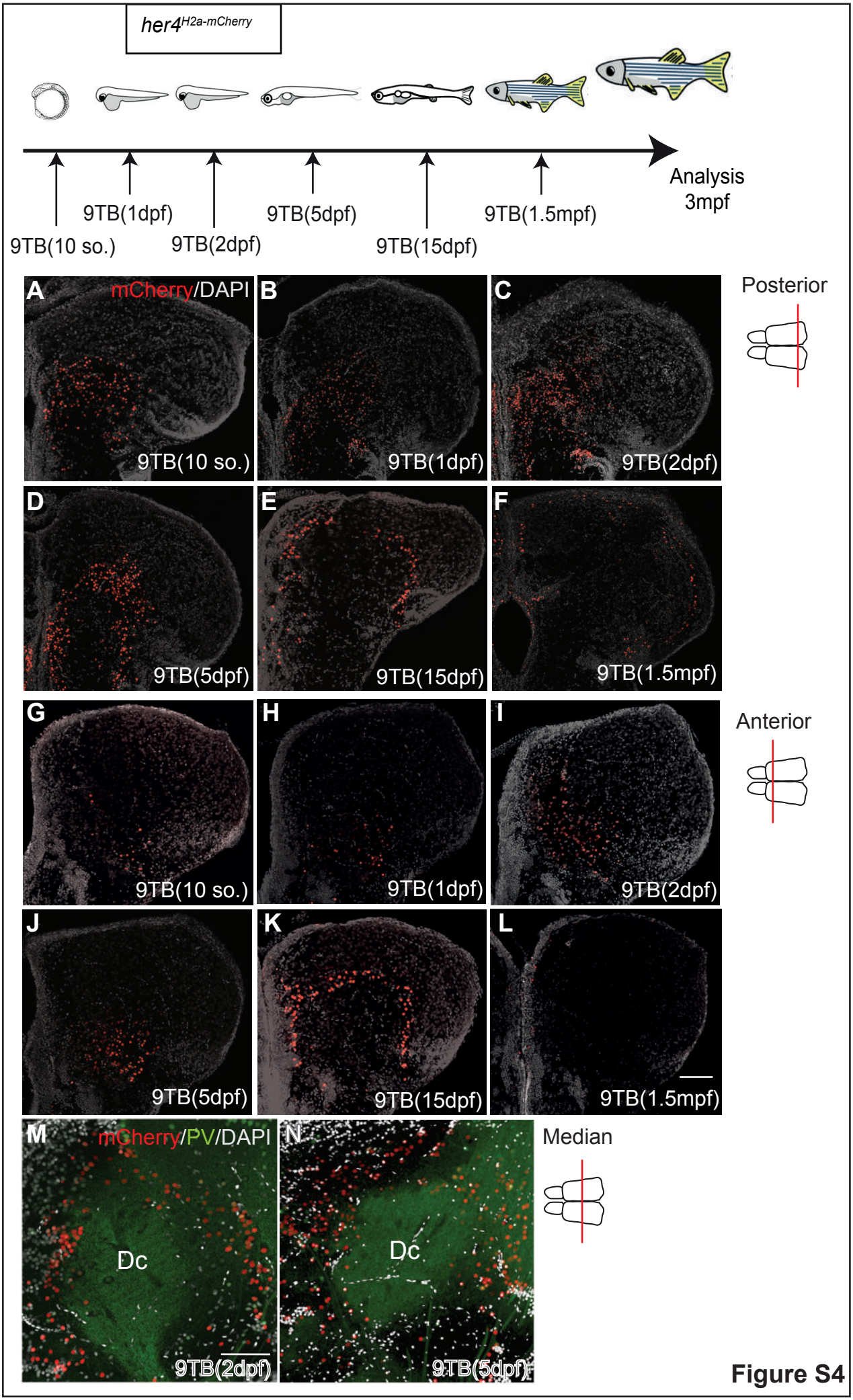
her4H2a-mCherry
Analysis
3mpf
9TB(10 so.)
9TB(1dpf)
9TB(2dpf)
9TB(5dpf)
9TB(15dpf)
9TB(1.5mpf)
A
mCherry/DAPI
9TB(10 so.)
B
9TB(1dpf)
C
9TB(2dpf)
Posterior
D
9TB(5dpf)
E
9TB(15dpf)
F
9TB(1.5mpf)
G
9TB(10 so.)
H
9TB(1dpf)
I
9TB(2dpf)
Anterior
J
9TB(5dpf)
K
9TB(15dpf)
L
9TB(1.5mpf)
M
mCherry/PV/DAPI
Dc
9TB(2dpf)
N
Dc
9TB(5dpf)
Median

Figure S4

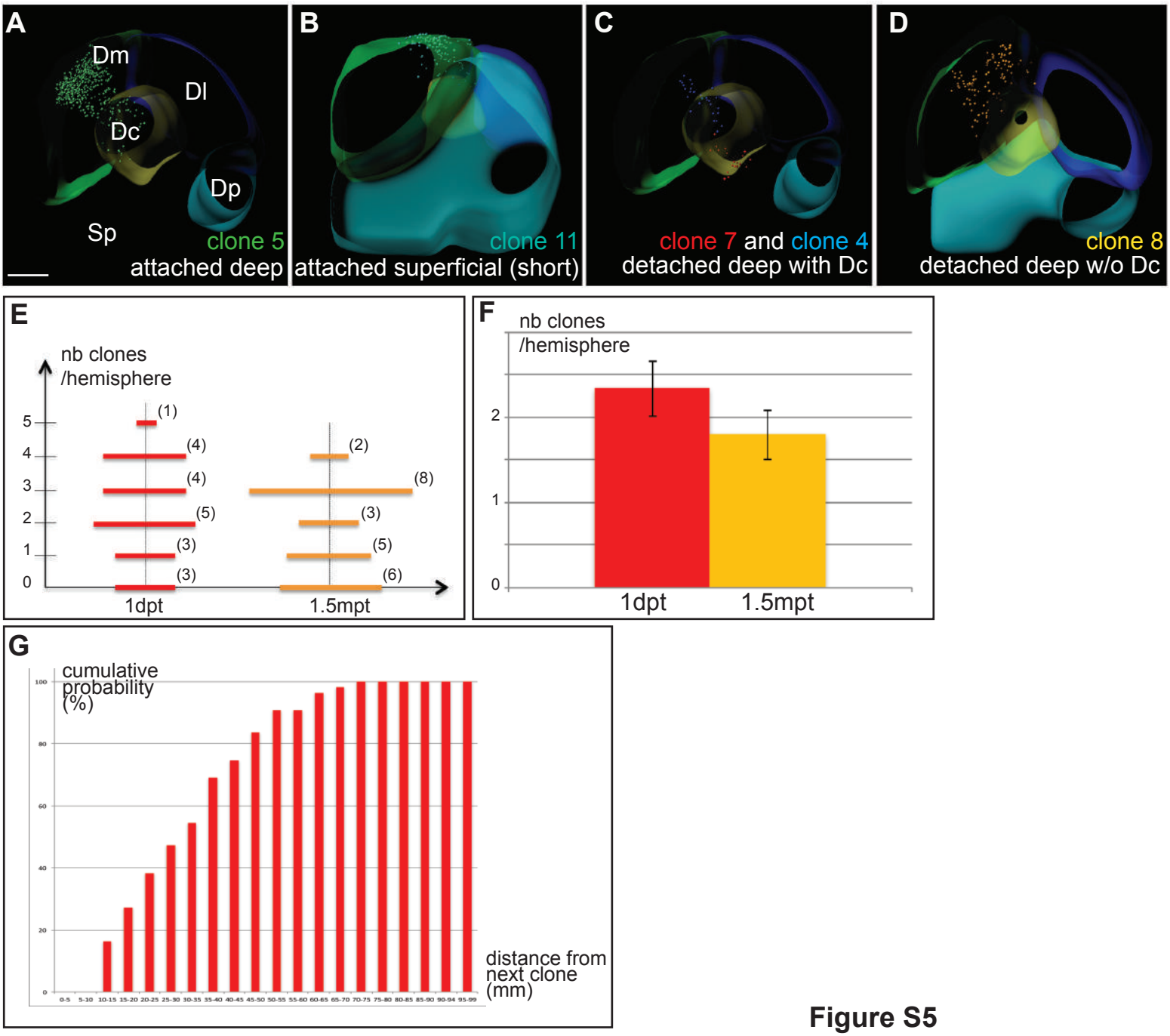
A
Dm
Dl
Dc
Dp
Sp
clone 5
attached deep
B
clone 11
attached superficial (short)
C
clone 7 and clone 4
detached deep with Dc
D
clone 8
detached deep w/o Dc
E
nb clones
/hemisphere
5
4
3
2
1
0
(1)
(4)
(4)
(5)
(3)
(3)
(2)
(8)
(3)
(5)
(6)
1dpt
1.5mpt
F
nb clones
/hemisphere
2
1
0
1dpt
1.5mpt
G
cumulative
probability
(%)
100
80
60
40
20
0
0-5
5-10
10-15
15-20
20-25
25-30
30-35
35-40
40-45
45-50
50-55
55-60
60-65
65-70
70-75
75-80
80-85
85-90
90-94
95-99
distance from
next clone
(mm)

Figure S5

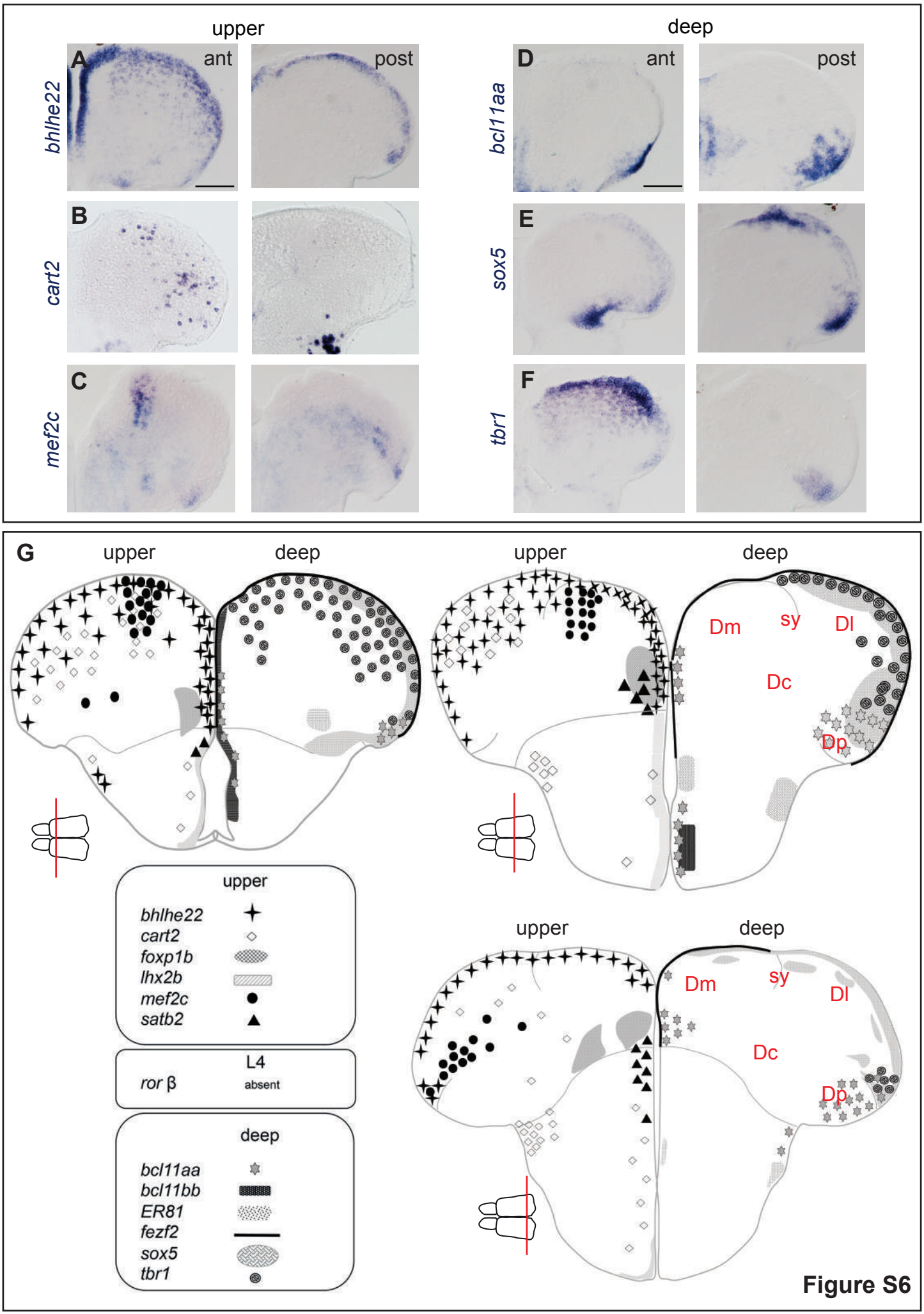
upper
deep
A
ant
post
bhlhe22
D
ant
post
bcl11aa
B
cart2
E
sox5
C
mef2c
F
tbr1
G
upper
deep
upper
deep
Dm
sy
Dl
Dc
Dp
upper
bhlhe22
cart2
foxp1b
lhx2b
mef2c
satb2
L4
ror β
absent
deep
bcl11aa
bcl11bb
ER81
fezf2
sox5
tbr1
upper
deep
Dm
sy
Dl
Dc
Dp

Figure S6

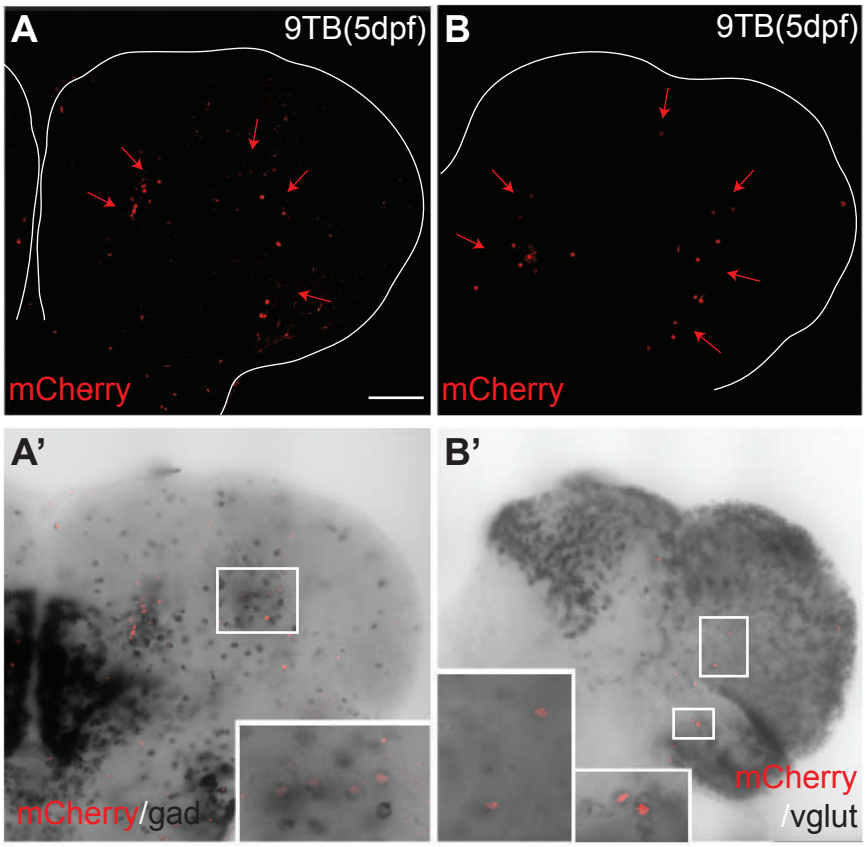
A
9TB(5dpf)
mCherry
B
9TB(5dpf)
mCherry
A'
mCherry/gad
B'
mCherry
/vglut

Figure S7

Figure S1 : **Eversion exposes the germinative RG layer in the adult zebrafish pallium,** related to Figure 1**. A.** Schematic representations of the neural stem cell (NSC)-dependent (**a, b**) and -independent (**c**) strategies shaping brain cytoarchitecture. The germinal NSC pool and its neurogenic activity are indicated in red, and neuronal identities issued from this pool are color-coded. The output structure is depicted at the top of each panel. (**a**) Continuous NSC activity generates age-related layers in the mammalian neocortex, in an inside-out fashion following radial neuronal migration. (**b, c**) Spatially controlled NSC activity and neuronal migration events organize functional nuclei in the bird and reptile neocortex (from [S4][S5]) **B.** Simplified schematized cross section of the zebrafish adult pallium at medial antero-posterior levels indicating the parenchymal subdivisions and sulci referred to in this study (from [S1]). The attachment point of the tela choroida, positioning the limit of the eversion process, is indicated (gray dots and arrows) (from [S2]). The pallial germinative zone (ventricular zone, red) extends from this point to the pallial-subpallial boundary (gray dashed line). **C.** Simplified schematized whole-mount view of the zebrafish adult pallium (viewed from top, anterior left) indicating the germinal zone areas visible from a dorsal view, as identified in [S3]. **D-G.** Whole-mount dorsal views of the pallial germinal zone in transgenic *her4:eGFP* telencephali, identified by the expression of GFP or GS (as indicated) at 2dpf (D), 5dpf (E), 1.5mpf (F) and 3mpf (adult, G). Whole-mount preparations counterstained with DAPI. Abbreviations: Da: anterior pallium; Dc: central pallium; Dl: lateral pallium domain; Dm: medial pallium domain; Dp: posterior pallium domain; ls: lateral sulcus; t.c.: tela choroida; sy: sulcus ypsiloniformis. Scale bars: D, E : 20μm; F : 50μm; G : 100μm.

Figure S2 : **Continuous and direct neurogenesis from radial glial (RG) cells in the zebrafish pallium from embryo to adulthood**, related to Fig.1. **A-E**. Cross sections of transgenic *her4:GFP* telencephali at 2dpf (**A**), 5dpf (**B**), 15dpf (**C**), 1.5mpf (**D**) and adult stage (**E**) at medial antero-posterior levels (see schemes on the right), immunostained for GFP or the RG marker Glutamine Synthase (green, left panel, as indicated), the proliferation marker PCNA (red, middle panel) and counterstained with DAPI (right panel). High magnifications in insets. White dashed line: position of the pallium/subpallium boudary. Scale bars: A, B inset, C inset : 20μm; D inset, E: 50μm. Abbreviations: Di: diencephalon; e: epiphysis; Hy: hypothalamus; Me: mesencephalon; ob: olfactory bulb; Sp: subpallium; Tel: telencephalon, V: ventricle.

Figure S3 : **Validation of the Tet-on strategy**, related to Fig.2. **A.** Compared expression of rtTA (*in situ hybridization*) and GS (immunocytochemistry) (color-coded, as indicated) on cross sections of the adult pallium in a *Tg(her4:rtTA)* fish (one hemisphere is shown, observed in

confocal microscopy). Note that *rtTA* and GS are expressed in the same set of ventricular RG. **B.** Proportion of mCherry-positive cells among ventricular cells at three different anteroposterior levels in *her4*$^{\text{H2a-mCherry, 9TB(5dpf)}}$ fish analyzed at 1 day-post-treatment (1dpt) (n=3 brains, T-test (α=0.05, not significant). **C.** Compared expression of the three reporters mCherry, Flag and GFP (immunocytochemistry, color-coded as indicated) observed in whole-mount pallia (C, D) or pallial cross sections at mid-anteroposterior levels (E-G) in double transgenic *Tg(her4:rtTA)*;*Tg(GFP:biTRE:H2amCHERRY*) fish induced with 9TB at 1dpf (C), 2dpf (D), 5dpf (E), 15dpf (F) and 1.5mpf (G) and sacrificed 1 day post-treatment (1dpt). Note the largely coincident expression of the three markers, the broader expression of mCherry being explained by the stability of the H2a-mCherry protein. Note also that, while *her4*-driven expression is limited to the pallial VZ until 5dpf (C-E), it extends to the subpallium at later stages (F, G). The red asterisk in panel G underlies a territory of the Dl VZ with low induction response at late stages (1.5mpf). The white line in E-G, right panels, indicates the pallial-subpallial boundary. Scale bars: C-E: 10µm; F, G: 50µm.

Figure S4 : **Zebrafish pallial neurogenesis follows a sequential stacking process : anterior and posterior analysis,** related to Fig.2. **A-L. Localization at posterior and anterior adult pallial levels of the mCherry-positive neurons born from *her4*-positive RG.** Position of mCherry-positive neurons on posterior (A-F) and anterior (G-L) 3mpf *her4*$^{\text{H2a-mCherry}}$ adult pallium cross sections observed in confocal microscopy (with DAPI counterstain) following 9TB induction at the stages indicated. **M, N. Localization, at median pallial levels, of the neurons born at 2 and 5dpf relative to Dc.** High magnification views of the confocal images shown in Fig.2C' and D', respectively, stained for mCherry and PV and counterstained with DAPI. Scale bars: 50µm.

Figure S5 : **Superimposed individual brainbow clones and neuroanatomical domains**, related to Figs.5 and 6. **A-D.** 5 clones are shown on thick cross sections of the brain shown in Fig.5A. Clone categories, as defined in Fig.5 C-G and Table S1, are indicated at the bottom right of each panel, and the clones illustrated are color-coded as in Fig.5C-I and Table S1. Note that clone n°5 and 7, shown in A and C respectively, reach into Dc. Scale bar: 80µm. **E-G. Validation of clonality in the analysis of *her4*$^{\textit{actswitch,T(5dpf)}}$ larvae**. **E.** Compared distribution of the number of induced progenitors at 1 day-post-9TB (1dpt) and the number of clones at 1.5mpf (1.5 months post 9TB –mpt-). n = 20 pallial hemispheres at 1dpt and 24 pallial hemispheres at 1.5mpt. The numbers in bracket indicate the number of hemispheres concerned for each number of induced cells/clone. **F.** Average number of induced progenitors per hemisphere at 1dpt or induced clones per hemisphere at 1.5mpt (averaged from panel E). sem: 0.32 at 1dpt, 0.28 at 1.5mpt. Difference

is not significant (P<0.25). **G.** Cumulative distribution of the nearest neighbors distances separating labeled progenitors in the pallium of a *her4*$^{H2a\text{-}mCherry,9TB(5dpf)}$ animal analyzed at 1dpt (Fig.6A, A'). 84% of induced clones are located at least 15μm (approx. 4 cell diameters) away from their nearest neighbor clone.

Figure S6 : **Expression in the adult zebrafish pallium of genes identifying neocortical layers in mammals and/or birds: other anteroposterior levels and summary schemes,** related to Fig.7 **A-F.** Anterior (left panels) and posterior (right panels) pallial cross sections from the specimen shown in Fig.7 (*in situ hybridization* for the indicated probes, blue signal), ordered here for gene probe orthology with markers of deep (left) or upper (right) layer neurons in other vertebrates (see Table S4). **G.** Schematic summary of the expression patterns, on cross sections of the adult zebrafish pallium at anterior, median and posterior levels (equivalent to Fig.7 and panels A-F), of all the genes tested in this study (Table S4). Scale bars: 100μm.

Figure S7 : **Compared localization of GABA and Glutamatergic neurons with the position of neurons born at 5dpf in the adult pallium,** related to Fig.7. **A-B'**: Cross-sections at median pallial levels of *her4*$^{H2a\text{-}mCherry,9TB(5dpf)}$ brains observed at 3mpf (confocal microscopy, single 70μm stacks), immuno-processed for mCherry and stained by *in situ hybridization* with the following probes: *gad65/67a/67b* (*gad*, A') and *vglut1/2.1/2.2* (*vglut*, B'). **A, B**: fluorescence channels; **A', B'**: superimposed bright field and fluorescence channels; red arrows in A, B indicate the shape of the mCherry-positive domains and white dotted lines line the pallial contour. Insets are high magnifications of the boxed areas showing mCherry in the nucleus of *gad*- or *vglut*-positive neurons. Scale bar: 70 μm.

A	B	C	D	E	F	G	H	I	J	K	L	M	N	O	P
Clone #	Nb cells	Nb neurons	Nb ventricular cells	Type	Clone length in depth (µm)	Clone width (µm)	Distance of clone from VZ (µm)	Neuroanatomical location (VZ)	Neuroanatomical location (depth)	A/P location	clone deepest z on cross section (µm)	pallium deepest z on cross section (µm)	deepest z / pallial z ratio in %	"deep" limit (table S2)	"Dc" limit (table S2)
5	654	415	238	Attached/Deep	411	238		Dm	Dc	middle	413	450	92	39	71
6	646	568	78	Attached/Deep	384	284		Dm	Dc	posterior	381	450	85	76	82
9	29	22	7	Attached/Deep	406	221		Dm	Dc	middle	458	554	83	39	71
10	398	307	91	Attached/Deep	394	256		Dm	Dc	posterior	394	450	88	76	82
13	120	87	33	Attached/Deep	528	102		Da	Dc	anterior	418	450	93	86	92
14	206	143	63	Attached/Deep	324	164		Dm	Dc	middle	445	554	80	39	71
15	606	380	226	Attached/Deep	512	255		Dm	Dc	posterior	393	450	87	76	82
16	367	265	102	Attached/Deep	491	105		Dm	Dc	middle	420	554	76	39	71
18	560	487	73	Attached/Deep	419	101		Da	Dc	anterior	548	583	94	86	92
20	215	190	25	Attached/Deep	348	85.5		Dm		middle	403	644	63	39	71
26	67	53	14	Attached/Deep	404	110		Dm		middle	520	805	65	39	71
29	192	158	34	Attached/Deep	391	90.7		Da		anterior	592	700	85	86	92
31	42	32	10	Attached/Deep	409	103		Dm		middle	532	805	66	39	71
32	108	70	38	Attached/Deep	325	101		Dm		middle	494	805	61	39	71
33	118	90	28	Attached/Deep	325	129		Dm		middle	503	805	62	39	71
34	133	81	52	Attached/Deep	387	97.5		Dm		middle	511	805	63	39	71
2	162	109	53	Attached/Superficial	394	220 (short)		Dm		posterior	278	554	50	76	82
3	68	52	16	Attached/Superficial	291	252 (short)		Dm		posterior	201	450	45	76	82
11	137	72	65	Attached/Superficial	243	282 (short)		Dm		posterior	171	450	38	76	82
17	304	220	84	Attached/Superficial	214	304 (flat)		Dm		middle	145	644	23	39	71
21	404	269	135	Attached/Superficial	283	436 (flat)		Dm		middle	195	644	30	39	71
22	67	110	21	Attached/Superficial	374	122 (short)		Da		anterior	454	583	78	86	92
23	501	371	130	Attached/Superficial	550	191 (short)		Dm		anterior	550	805	68	86	92
28	139	96	43	Attached/Superficial	498	127 (short)		Dm		posterior	489	805	61	76	82
30	38	28	10	Attached/Superficial	186	85.4 (short)		Dm		middle	236	805	29	39	71
25	144	99	45	Attached	230	79.3 (short)		Dl		middle	230	805	29	39	71
27	247	187	60	Attached	384	117		Dl		anterior	489	700	70	86	92
4	28	28	0	Detached/Deep			160	Dm	Dc	middle	433	450	96	39	71
7	21	21	0	Detached/Deep			425	Dm	Dc	middle	545	554	98	39	71
19	473	473	0	Detached/Deep			254	Dm	Dc	middle	468	644	73	39	71
1	25	25	0	Detached/Deep			123	Dm		middle	339	554	61	39	71
8	119	119	0	Detached/Deep			61	Dm		middle	358	554	64	39	71
12	89	89	0	Detached/Deep			217	Dm		middle	385	554	69	39	71
24	82	82	0	Detached/Deep			218	Dm		middle	391	805	49	39	71

Total clone nb		34			
Attached	27 (80%)	Deep	16 (64%)	Including Dc	9
		Superficial	9 (36%)	Short	7
				Flat	2
		ND	2		
Detached	7 (20%)	Deep	7 (100%)	Including Dc	3
		Superficial	0		

Table S1

A/P section level	anterior			middle			posterior		
9-TB timing	deepest z on cross section (µm)	pallial z on cross section (µm)	deepest z / pallial Z ratio in %	deepest z on cross section (b, in µm)	pallial z on cross section (a, in µm)	deepest z / pallial Z ratio in %	deepest z on cross section (µm)	pallial z on cross section (µm)	deepest z / pallial Z ratio in %
Figure 4, Table S1									
24hpf	500	510	98	355	395	90	380	410	93
48hpf	510	550	**92**	250	350	**71**	329	402	**82**
5dpf	479	559	**86**	136	345	**39**	301	396	**76**
15dpf	280	507	55	67	360	18	244	398	61
1.5mpf	20	461	4	17	370	5	34	410	8
"deep" limit			**86**			**39**			**76**
Dc limit			**92**			**71**			**82**

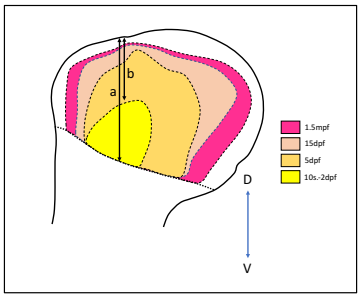

Table S2

A	B	C	D	E	F	G	H	I	J	K	L	M	N	O	P
Clone #	Nb cells	Nb neurons	Nb RG (GS+)	Nb proliferating RG (GS+, PCNA+)	Nb proliferating precursors (GS-, PCNA+)	**Type**	Clone length in depth (µm)	Long axis of VZ area (µm)	Short axis of VZ area (µm)	Distance of clone from VZ (µm)	**Neuroanatomical location (VZ)**	**A/P location**	clone deepest z on cross section (µm)	pallium deepest z on cross section (µm)	deepest z / pallial Z ratio (in %)
1	37	33	0	4	0	**Attached**	122	19	10	0	**Da**	**middle**	118	130	91
2	47	38	0	3	6	**Attached**	119	15	1 row	0	**Da**	**anterior**	82	130	63
3	49	44	5	0	0	**Attached**	53	20	12	0	**Dl**	**middle**	52.5	130	40
5	56	53	3	0	0	**Attached**	92	21	1 row	0	**Dp**	**posterior**	46.5	130	36
6	11	6	4	1	0	**Attached**	12	22,1	1 row	0	**Da**	**anterior**	16.8	130	13
7	99	90	9	0	0	**Attached**	66	52	20	0	**Dl**	**posterior**	62.4	120	52
8	176	148	28	0	0	**Attached**	45	57	26	0	**Da**	**anterior**	35.3	120	30
9	39	38	1	0	0	**Attached**	45	1 GS cell only	NR	0	**Dm**	**middle**	45.3	120	38
10	31	27	3	1	0	**Attached**	17	7	1 row	0	**Dm**	**middle**	53.6	120	45
11	48	42	6	0	0	**Attached**	34	31	21	0	**Dm**	**middle**	17.9	90	20
14	48	41	0	4	3	**Attached**	31	28	12	0	**Dm**	**middle**	33.7	112	30
15	28	26	2	0	0	**Attached**	60	17	1 row	0	**Dl**	**posterior**	49.2	112	44
16	42	38	4	0	0	**Attached**	38	23	4	0	**Dp**	**posterior**	45.6	112	41
17	71	62	9	0	0	**Attached**	80	32	17	0	**Da**	**anterior**	69.8	112	62
19	104	94	10	0	0	**Attached**	252	31	18	0	**Da**	**anterior**	94.8	95,8	99
20	76	ND	ND	ND	ND	**Attached**	148	ND	ND	0	**Dm**	**middle**	61.5	95,8	64
21	176	142	34	0	0	**Attached**	100	82	30	0	**Da**	**middle**	76.6	95,8	80
22	201	160	7	6	28	**Attached**	86	22	8	0	**Dl**	**posterior**	80.7	95,8	84
23	16	ND	ND	ND	ND	**Attached**	41	ND	ND	0	**Dm**	**middle**	74.9	90	83
24	99	ND	ND	ND	ND	**Attached**	127	ND	ND	0	**Da**	**anterior**	126	130	97
25	134	ND	ND	ND	ND	**Attached**	97	ND	ND	0	**Dp**	**posterior**	48.2	130	37
26	79	33	6	2	38	**Attached**	133	36	14	0	**Dp**	**posterior**	79	130	61
27	27	23	1	2	1	**Attached**	43	16	1 row	0	**Dp**	**posterior**	47	110	43
28	26	23	0	3	0	**Attached**	69	10	1 row	0	**Dm**	**middle**	37	110	34
29	49	46	2	1	0	**Attached**	61	14	1 row	0	**Dp**	**posterior**	43.8	110	40
30	41	31	1	2	7	**Attached**	31	16	1 row	0	**Dm**	**middle**	17.3	110	16
31	24	17	5	2	0	**Attached**	31	17	11	0	**Dm**	**middle**	45.1	110	41
32	37	36	1	0	0	**Attached**	65	1 GS cell only	NR	0	**Dp**	**posterior**	57.7	106	54
33	41	36	3	2	0	**Attached**	42	19	1 row	0	**Dm**	**middle**	22.4	106	21
34	53	34	18	0	1	**Attached**	48	51	19	0	**Dm**	**middle**	38.4	106	36
35	69	ND	ND	ND	ND	**Attached**	113	ND	ND	0	**Dp**	**posterior**	23.8	104	23
36	47	42	5	0	0	**Attached**	88	23	1 row	0	**Dm**	**middle**	25.5	70,4	36
37	38	35	3	0	0	**Attached**	39	15	8	0	**Dm**	**middle**	42	105	40
38	54	44	9	1	0	**Attached**	33	35	18	0	**Dm**	**middle**	33.6	105	32
39	23	11	12	0	0	**Attached**	42	25	12	0	**Da**	**anterior**	52	105	50
40	71	60	9	1	1	**Attached**	86	29	15	0	**Da**	**anterior**	76.6	105	73
4	33	33	0	0	0	**Detached**	74	NR	NR	10	**Dm**	**middle**	67.9	130	52
12	8	8	0	0	0	**Detached**	35	NR	NR	9	**Dm**	**middle**	26.8	90	30
13	19	19	0	0	0	**Detached**	71	NR	NR	22	**Dl**	**posterior**	74.8	90	83
18	5	5	0	0	0	**Detached**	75	NR	NR	37	**Dm**	**posterior**	107	130	82

Total clone nb	**40**
Attached	**36 (90%)**
Detached	**4 (10%)**

Table S3

Gene	Rodents	Human	Birds	Zebrafish ortholog(s)	Adult zebrafish pallium (>2mpf)	refs
bhlhe22(bhlhb5)	L2-L5			*bhlhe22(bhlhb5)**	active / recent neurogenesis zones	[S7]
Cux2	L2-L3	L2 (and L4)	mesopallium	*cux2a*, cux2b*	no expression	[S4], [S5]
Cart	L5	L2-3		*cart1, cart2*, cart3, cart4*	salt and pepper	[S15]
FoxP1	L3-L6 in embryos, L4-L5 in adult	L3-L6	mesopallium	*foxp1a, foxp1b**	stripe, ventral Dm (neurons)	[S4], [S8]
Lhx2	L3-L4			*lhx2a, lhx2b**	neurogenesis zone in ventral Dm	[S3]
Mef2c	L2 in embryos, L2-6 in adult	L2-L3-L4	mesopallium, nidopallium	*mef2c**	sub-domain in Dm	[S4], [S5], [S13]
Satb2	L2 in embryos, L2-6 in adult	L5	mesopallium	*satb2**	almost no expression (subpallium only)	[S4], [S5], [S8]
Ror β	L4	L4	thal. recipient (entopallium, field L)	*ror β**	no expression (midbrain only)	[S4]
Eag2/Kcnh5	L4		thal. recipient, entopallium	*kcnh5a, kch5b*		[S4]
*CTIP1**	L1 in embryos, all layers at postnatal stages			*bcl11aa**	sub-domain in Dl/Dp, active neurogenesis zone in ventral Dm	[S10]
CTIP2	L5 in embryos, L4-L6 in adult	L5b	medial domains chick pallium, parahippocampal area	*blc11bb**	subpallium	[S8], [S9]
ER81	L5	L5	arcopallium, parahippocampal area	*ER81**	no expression (subpallium only)	[S4], [S5]
Fezf2	L5	L5b	parahippocampal area	*fezf2**	active neurogenesis zone	[S4], [S11]
Sox5	L5-L6	L6		*sox5**	active / recent neurogenesis zones	[S12]
Sulf2	L5			*sulf2a,b*		[S4]
Tbr1	L6	L5-L6		*tbr1**	active / recent neurogenesis zones	[S14]

Table S4

Table S1. Quantitative characteristics of the clones segmented in *her4*$^{Zebrabow,T(1dpf)}$ adult pallia. **Column A** : clone numbers, see Fig.5 and Fig.S5 for illustrations of the clones highlighted in color. **Columns B-D** : total number of cells per clone (B), as the sum of the number of neurons (C) and ventricular cells (D). **Column E** : clone type. "Attached" clones are defined as possessing at least one ventricular (progenitor) cell, while "detached" clones have no ventricular cells. The clones are further classified as "deep" if they contain neurons born at or before 5dpf, and as "superficial" otherwise. The z positions of the 5dpf ("deep") and Dc (48hpf) limits (**columns O and P**) were measured on standard anterior, middle or posterior sections as in Figs.2 and S4, and normalized by pallial depth at these antero-posterior positions (Table S2). These limits are here compared to the ratio of the "z position of the deepest clone cell" to "pallial depth" for each clone (**columns L-N**) to estimate the age of the first-born neuron of each clone. Due to the curvature of the age-related neuronal sheets (eg. see Fig.2G), the age of clones situated laterally could not be ascertained and these clones are only referred to as "attached" (clones 25 and 27). **Columns F-G** : total length (distance from the most superficial to the deepest cell, F) and width (largest measure parallel to the VZ plane, G) of each clone; attached clones are referred to as "flat" if their width is superior to their length; they are referred to as "short" otherwise. **Column H** : in the case of "detached" clones, distance of the most superficial cell to the ventricular surface. **Columns I-J** : neuroanatomical location of the clone at the ventricular zone (I, Da, Dm, Dl or Dp) and in depth (J, clone overlapping – green- or not Dc). **Column K** : antero-posterior location of the clone along the pallium. "Anterior", "middle" and "posterior" levels are those illustrated in Figs.2 and S4 and measured in Table S2. **Bottom table**: total count of the different clone categories, as defined above.

Table S2. Quantitative positioning of neurons born at the indicated ages on anterior, middle and posterior cross sections of the pallium at 3mpf. The position of sections is as shown in Figs.2 and S4. The diagnostic "age ratio" (deepest z/pallial at anterior, middle and posterior level) is obtained by normalizing the z position of the deepest H2a-mCherry-positive neurons (value "b" on the scheme) by the deepest z position of the pallium (value "a" on the scheme). Values in bold are those reported into Table S1.

Table S3. Quantitative characteristics of the clones segmented in *her4*$^{actswitch,T(5dpf)}$ 1.5 mpf pallia. See Fig.6 for illustrations. **Column A :** clone numbers (see Fig.6 for illustrations). **Columns B-F :** number of cells of each type within clones (number of neurons (column C), number of quiescent radial glia (GS-positive, PCNA-negative) (column D), number of activated radial glia (GS-positive, PCNA-positive) (column E) and number of proliferating non-glial precursor (GS-negative, PCNA-positive) (column F)). **Column G :** clone types (only classified as "attached" or "detached" in this

experiment). **Column H :** Clone length (length of longest axis in the parenchyme). **Columns I, J:** Size (length, width) of the VZ component (RGs, aNPs) of each clone along the ventricular plane (see Fig.6E for the schematic representation of each category –the short axis can be composed of several cell rows, one cell row, or no cells if the VZ component only consists in 1 cell-). **Column K:** depth of the clone within the parenchyme (for detached clones). **Column L** : neuroanatomical location of the clone at the ventricular zone (I, Da, Dm, Dl or Dp). **Column M** : antero-posterior location of the clone along the pallium. Columns N-P: Deepest positions of each clone and of the pallium on cross-sections, and corresponding ratios. **Bottom table** : total count of the 2 clone categories defined above. ND: not determined; NR: not relevant.

Table S4. List of the genes identifying neocortical layers in mouse, human and chick used in this study. The zebrafish orthologs are identified, and expression profiles in each case are reported. In case expression differs between embryonic and adult stage in rodents, this is also indicated. Zebrafish genes selected for illustrations in Figs.7 and S6 are indicated with an asterisk. After references [S5][S6][S4][S7][S8][S9][S10][S11][S12][S13][S14][S15].

Abbreviations list

Da anterior subdivision of the pallial ventricular zone

Dc central subdivision of the pallium

Dl lateral subdivision of the pallium

Dm medial subdivision of the pallium

Dp posterior subdivision of the pallium

NPC neural progenitor cell

NSC neural stem cell

PV Parvalbumin

RG radial glia

sy sulcus ypsiloniformis

VZ ventricular zone

References

S1. Wullimann, M.F., Rupp, B., and Reichert, H. (1996). Neuroanatomy of the Zebrafish Brain: A Topological Atlas

S2. Nieuwenhuys, R. (2011). The development and general morphology of the telencephalon of actinopterygian fishes: Synopsis, documentation and commentary. Brain Struct. Funct. *215*, 141–157.

S3. Dray, N., Bedu, S., Vuillemin, N., Alunni, A., Coolen, M., Krecsmarik, M., Supatto, W., Beaurepaire, E., and Bally-Cuif, L. (2015). Large-scale live imaging of adult neural stem cells in their endogenous niche. Development *142*, 3592–600.

S4. Suzuki, I.K., Kawasaki, T., Gojobori, T., and Hirata, T. (2012). The Temporal Sequence of the Mammalian Neocortical Neurogenetic Program Drives Mediolateral Pattern in the Chick Pallium. Dev. Cell *22*, 863–870.

S5. Dugas-Ford, J., Rowell, J.J., and Ragsdale, C.W. (2012). Cell-type homologies and the origins of the neocortex. Proc. Natl. Acad. Sci. U. S. A. *109*, 16974–9.

S6. Dugas-Ford, J., and Ragsdale, C.W. (2015). Levels of Homology and the Problem of Neocortex. Annu. Rev. Neurosci. *38*, 351–68.

S7. Joshi, P.S., Molyneaux, B.J., Feng, L., Xie, X., Macklis, J.D., and Gan, L. (2008). Bhlhb5 Regulates the Postmitotic Acquisition of Area Identities in Layers II-V of the Developing Neocortex. Neuron *60*, 258–272.

S8. Cobos, I., and Seeley, W.W. (2015). Human von economo neurons express transcription factors associated with Layer v subcerebral projection neurons. Cereb. Cortex *25*, 213–220.

S9. Arlotta, P., Molyneaux, B.J., Chen, J., Inoue, J., Kominami, R., and MacKlis, J.D. (2005). Neuronal subtype-specific genes that control corticospinal motor neuron development in vivo. Neuron *45*, 207–221.

S10. Woodworth, M.B., Greig, L.C., Liu, K.X., Ippolito, G.C., Tucker, H.O., and Macklis, J.D. (2016). Ctip1 Regulates the Balance between Specification of Distinct Projection Neuron Subtypes in Deep Cortical Layers. Cell Rep. *15*, 999–1012.

S11. Berberoglu, M.A., Dong, Z., Mueller, T., and Guo, S. (2009). fezf2 expression delineates cells with proliferative potential and expressing markers of neural stem cells in the adult zebrafish brain. Gene Expr. Patterns *9*, 411–422.

S12. Ip, B.K., Bayatti, N., Howard, N.J., Lindsay, S., and Clowry, G.J. (2011). The corticofugal neuron-associated genes ROBO1, SRGAP1, and CTIP2 exhibit an anterior to posterior gradient of expression in

early fetal human neocortex development. Cereb. Cortex *21*, 1395–1407.

S13. Leifer, D., Li, Y.L., and Wehr, K. (1997). Myocyte-specific enhancer binding factor 2C expression in fetal mouse brain development. J Mol Neurosci *8*, 131–143.

S14. Hevner, R.F., Shi, L., Justice, N., Hsueh, Y.P., Sheng, M., Smiga, S., Bulfone, A., Goffinet, A.M., Campagnoni, A.T., and Rubenstein, J.L.R. (2001). Tbr1 regulates differentiation of the preplate and layer 6. Neuron *29*, 353–366.

S15. Lein, E.S., Hawrylycz, M.J., Ao, N., Ayres, M., Bensinger, A., Bernard, A., Boe, A.F., Boguski, M.S., Brockway, K.S., Byrnes, E.J., *et al.* (2007). Genome-wide atlas of gene expression in the adult mouse brain. Nature *445*, 168–176.